



## Supercapacitor and supercapattery as emerging electrochemical energy stores

George Z. Chen

To cite this article: George Z. Chen (2016): Supercapacitor and supercapattery as emerging electrochemical energy stores, International Materials Reviews, DOI: [10.1080/09506608.2016.1240914](https://doi.org/10.1080/09506608.2016.1240914)

To link to this article: <http://dx.doi.org/10.1080/09506608.2016.1240914>



© 2016 The Author(s). Published by Informa UK Limited, trading as Taylor & Francis Group



Published online: 17 Oct 2016.



Submit your article to this journal [↗](#)



Article views: 283



View related articles [↗](#)



View Crossmark data [↗](#)

FULL CRITICAL REVIEW



## Supercapacitor and supercapattery as emerging electrochemical energy stores

George Z. Chen <sup>a,b,c</sup>

<sup>a</sup>Department of Chemical and Environmental Engineering, Faculty of Engineering, University of Nottingham, Nottingham, UK; <sup>b</sup>Department of Chemical and Environmental Engineering, Faculty of Science and Engineering, University of Nottingham Ningbo China, Ningbo, PR China; <sup>c</sup>Centre for Sustainable Energy Technologies, Faculty of Science and Engineering, University of Nottingham Ningbo China, Ningbo, PR China

### ABSTRACT

This article reviews critically selected recent literature on electrochemical energy storage (EES) technologies, focusing on supercapacitor and also supercapattery which is a generic term for various hybrid devices combining the merits of rechargeable battery and supercapacitor. Fundamentals of EES are explained, aiming at clarification of some literature confusions such as the differences between capacitive and non-capacitive Faradaic charge storage mechanisms, and between cathode and positive electrode (positrode), and between anode and negative electrode (negatrode). In particular, the concept and origin of pseudocapacitance are qualitatively correlated with the band model for semiconductors. Strategies for design and construction of supercapattery are discussed in terms of both the materials structures and device engineering. Selection of materials, including electrolytes, is another topic reviewed selectively. Graphenes and carbon nanotubes are the favourable choice to composite with both capacitive and non-capacitive redox materials for improved kinetics of charge storage processes and charge–discharge cycling stability. Organoaqueous electrolytes show a great potential to enable EES to work at sub-zero temperatures, while solid ion conducting membranes and ionic liquids can help develop high voltage (>4.0 V) and hence high energy supercapatteries.

### ARTICLE HISTORY

Received 5 November 2015  
Accepted 20 September 2016

### KEYWORDS

Supercapattery; supercapacitor; capacitive and non-capacitive faradaic processes; nanocomposite; organoaqueous and non-aqueous electrolytes; device engineering

## Introduction

Harvesting energy from the unlimited but intermittent renewable sources such as sunlight, wind and tide demands efficient and affordable energy storage technologies. The diversity of energy forms and applications also means that development of such technologies must take an approach with multiple vectors. Electrochemical energy storage (EES) technologies together with materials development are currently playing leading and promising roles in the global effort to tackle the challenges to sustain energy supply [1,2]. In particular, materials and technological innovations based on electrochemical reactions and capacitance are being increasingly recognised and utilised to develop, respectively, rechargeable batteries with high energy capacity, and supercapacitors (also known as electrochemical capacitors) with high power capability and long cycle life measured against the common ground [3,4]. The past two decades have seen significant progresses in both rechargeable battery and supercapacitor research, although each alone is still unsatisfactory according to commercial

views that have been formed on consumption of fossil fuels. This situation calls for innovative changes in the research and development of EES technologies, leading to the proposal and preliminary demonstration of several hybrid devices that combines both the rechargeable battery and supercapacitor characteristics into one device, namely supercapattery whose behaviour is similar to that of a supercapacitor with a greater energy capacity, and supercabattery which performs more like a rechargeable battery but higher power capability and/or longer charge–discharge durability [5–8].

This article intends to offer a critical review of the research development in the past two decades in relation to understanding and improvement of supercapacitors, and of the very recently proposed hybrids of rechargeable battery and supercapacitor, particularly supercapattery. The focus will be on supercapacitor and supercapattery, and the associated nanostructured, redox active, and semiconductor materials such as electronically conducting polymers (ECPs) and transition metal oxides (TMOs). As a new EES device,

**CONTACT** George Z. Chen  george.chen@nottingham.ac.uk  Department of Chemical and Environmental Engineering, Faculty of Engineering, University of Nottingham, Nottingham NG7 2RD, UK

© 2016 The Author(s). Published by Informa UK Limited, trading as Taylor & Francis Group.

This is an Open Access article distributed under the terms of the Creative Commons Attribution License (<http://creativecommons.org/licenses/by/4.0/>), which permits unrestricted use, distribution, and reproduction in any medium, provided the original work is properly cited.

supercapattery aims to achieve comparable performance to supercapacitor in power capability and cycle life, and to battery in energy capacity. It can be achieved by hybridisation of either materials or electrodes in the same device. The material approach emphasises on the design and synthesis of hybrid or composite of a supercapacitor electrode material and a battery electrode material, and the use of such a hybrid material to make the electrode for use in the EES device. For example, the hybrid material of carbon nanotubes (CNTs) (which can be used alone as a supercapacitor electrode material) and manganese dioxide (which is a classic electrode material for battery) offers much higher specific charge capacity (or capacitance) than CNTs, and significantly greater specific power and longer cycle life than manganese dioxide. At the device level, combination of a supercapacitor electrode with a battery electrode in the same EES device can also

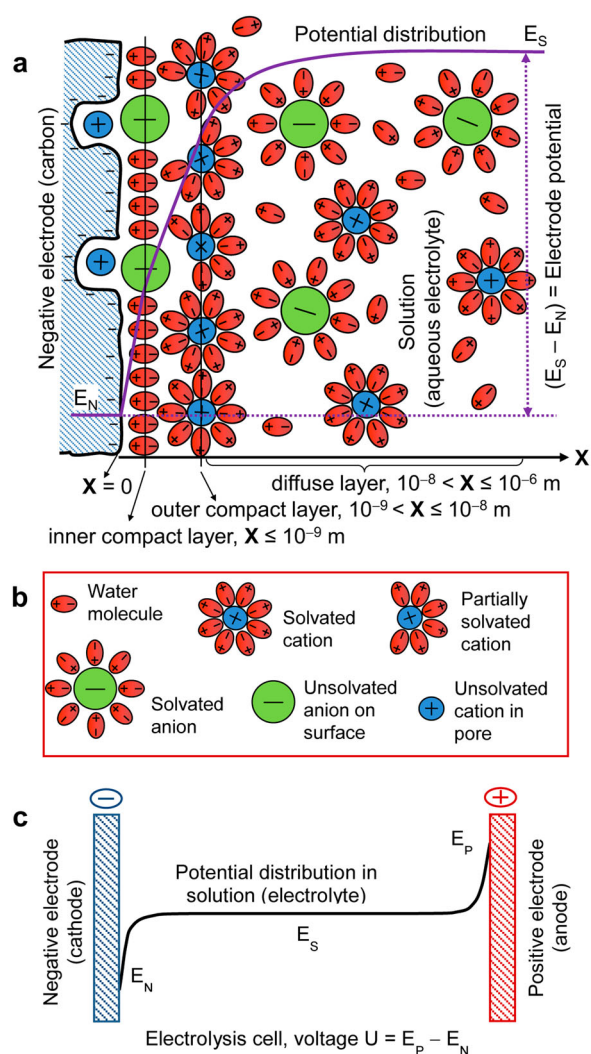


**Figure 1.** Schematic representations of (a) the EDL structure (cross-section) of the interface between a porous carbon negative electrode and an aqueous electrolyte; (b) explanations of symbols in (a); (c) potential distribution in the electrolyte solution between the negative and positive electrodes in an electrolysis cell. In (a, c),  $E_N$ ,  $E_P$  and  $E_S$  are respectively the potentials of the negative and positive electrodes, and the electrolyte sufficiently farther away from the electrode surface [15].

be effective for gaining performance improvement. This approach is simpler in concept, but challenging in practice in terms of matching the dissimilar performances of the two electrodes. In comparison with the material approach, only a few very successful laboratory studies have been reported recently via the device approach [5–8].

It is worth pointing out that several terms are used in the literature to describe hybrid EES devices, such as ‘redox capacitors’, and ‘Li-ion capacitors’, ‘pseudocapacitors’ and ‘Li-ion capacitors’ [9–14]. In an industrial EES project initiated in 2007, the author and collaborators proposed to design and build the supercapattery as a third generation EES device [5]. This project and a few others under different names as mentioned above progressed concurrently, targeting on similar goals: development of more advanced hybrid EES devices from combination of the merits of supercapacitors and rechargeable batteries. In the past decade, many review articles have discussed investigations on hybrid materials, but few accounted for device designs and engineering. Also, research progresses from different angles have come to the point calling for a unified generic term to describe these hybrid devices that are different from either supercapacitors or batteries in terms of fundamental principles and technological prospects.

With both the terms of supercapacitor and supercapattery in the title, this review aims to present and discuss a number of relevant issues, including fundamentals of interfacial (or electric double layer (EDL)) capacitance and pseudocapacitance, synthesis of nanostructured hybrid (or composite) materials, charge transfer reactions at nanometre scales, selection of electrolytes in terms of storage needs. In addition, the importance of electrode and device engineering is highlighted with several examples in which the specific energy and power of the supercapattery have matched with or gone over that of the lithium ion battery. The prospects of supercapattery development are speculated based on materials and engineering advantages, highlighting the theoretical and practical feasibilities of using this new EES device to complement, or even replace in some cases, rechargeable battery and supercapacitor.

## Basics of EES

The term of ‘electrochemical energy storage’ (EES) has been popular in the literature since more than a decade ago, and it is comparable with, but *not identical* to the traditional term of ‘electrochemical energy conversion and storage’ which emphasises ‘conversion between electrical and chemical energy’. This is because currently popular EES technologies include three main types: (1) rechargeable batteries, including redox flow batteries, (2) electrochemical capacitors which are more widely known as supercapacitors, and (3) various hybrids of battery and supercapacitor which are called

supercapattery and supercabattery in this article. One type of supercapacitors called ‘electrical double layer capacitor’ (EDLC) can in principle directly store electrical energy. The charge storage occurs via electrostatic adsorption of ions at the interface between the electrode and electrolyte under an applied cell voltage, and proceeds simultaneously on both the positive and negative electrodes, but no chemical reaction occurs. Thus, electrical energy storage in the EDLC is widely considered to be physical in nature. Nevertheless, ions are always solvated in the bulk electrolyte solution, but less so when adsorbed at the ‘electrode | electrolyte’ interface (or in the EDL) as illustrated in Figure 1(a and b) for a porous carbon negative electrode in contact with an aqueous electrolyte. (*Note:* Many schematic illustrations of the EDL on a planar electrode surface exist in the literature, such as that given in Bard and Faulkner [15], while Figure 1(a) is for the EDL on a porous carbon negative electrode.) Therefore, charge storage in the EDLC still involves changes in chemical bonding, and hence is not purely physical, nor solely chemical.

The EDL has in fact a multi-layer structure, including the inner compact layer, outer compact layer and diffuse layer which is next to the bulk electrolyte solution (not shown in Figure 1(a)). Both cations and anions are solvated (or hydrated) in the diffuse layer (and bulk solution), but as shown in Figure 1(a), in the compact layers, the anions are unsolvated and specifically adsorbed on the surface of the negative electrode. Also, some cations are partially solvated or unsolvated due to interactions with the anions and the electrode surface and pores. It is worth pointing out that because of the close packing of ions on the electrode surface, the potential distributions in the inner and outer compact layers are both linear but different in gradient (or slope). In the diffuse layer, ion concentration and hence the potential profiles are deviating from linearity and reaching a plateau at the end next to the bulk solution. The potential profile of the whole cell is schematically shown in Figure 1(c). Note that the potential,  $E_S$ , in the bulk electrolyte remains almost constant because of the high mobility of ions. Also, in Figure 1(c), the potential profiles near the two electrodes are a little exaggerated to highlight the potential variation.

All EES devices are composed of a positive electrode, a negative electrode and an electrolyte separator, as illustrated in Figure 2(a). These components are packed in one or another way in a cell (i.e. the EES device). The electrolyte separator, which is the separator membrane in Figure 2(a), can be a liquid (typically the sulphuric acid solution in lead-acid battery), a solid (such as the sodium ion conducting beta-alumina membrane in the ZEBRA battery), or more commonly a porous membrane filled with a liquid electrolyte (for example, the glass fibre or gel membrane in supercapacitors). The positive and negative electrodes are made

of materials of high electronic conductivity, including various metals, carbons, ceramics and their composites with polymers. The electrodes are used in two ways in EES devices. First, the electronic conductor is used mainly for loading an active material for charge storage by coating or another method. This case applies to both rechargeable batteries and supercapacitors, and the electronically conducting substrate is called current collector which should be chemically and electrochemically inert in the cell environment. The other use of electrode is to conduct electrons from or into the redox active ions or molecules in the electrolyte and this case is common in redox flow batteries.

In quite many publications on EES, the positive electrode is also called as the cathode, while the negative electrode as the anode [1,2,14,16]. Figure 3 shows an example. Such uses of the cathode and anode terminology in any EES devices deviate from both electrical and electrochemical principles and also the device manufacturer’s instruction, and hence can be confusing or misleading. Positive and negative electrodes are based on their electrical polarities, i.e. the positive electrode always has a higher (or more positive) potential than the negative electrode. The current always flows from the positive to the negative electrode via the external circuit, and the electrons flow in the opposite direction. However, cathode and anode are defined, respectively, by the electrode reaction being reduction (i.e. the active material or molecule accepts electrons from the current collector) or oxidation (the active material or molecule losses electrons to the current collector). By calling an electrode as the cathode, it is impossible to know if its potential is higher or lower than that of the anode. The use of the cathode and anode notions in EES literature may be related with primary battery studies which have emphasised on the discharging behaviour. These notions may be thus followed in the early days of secondary battery research when discharging performance was more important than the efficiency of energy storage. It is also possible that the one-word terms (i.e. cathode and anode) are more convenient to write than the two-word terms (i.e. positive electrode and negative electrode).

However, both charging and discharge performances are crucial in the present global effort to develop efficient EES technologies and, for example, it is obviously confusing and inappropriate to describe the charging process of the lithium ion battery by stating the following: ‘During charging of the cell,  $\text{Li}^+$  ion reduction on the anode of carbon enclosed silicon nanowires caused less volume expansion’. Figure 3(b) explains another erroneous derivation from using the anode and cathode terminology. Many other similar problems exist, but all can be avoided by using the notions of positive and negative electrodes. It is interesting to mention that in ESS literature published in China in Chinese, positive and negative electrodes (正极 and 负极) are always the terms used, but the

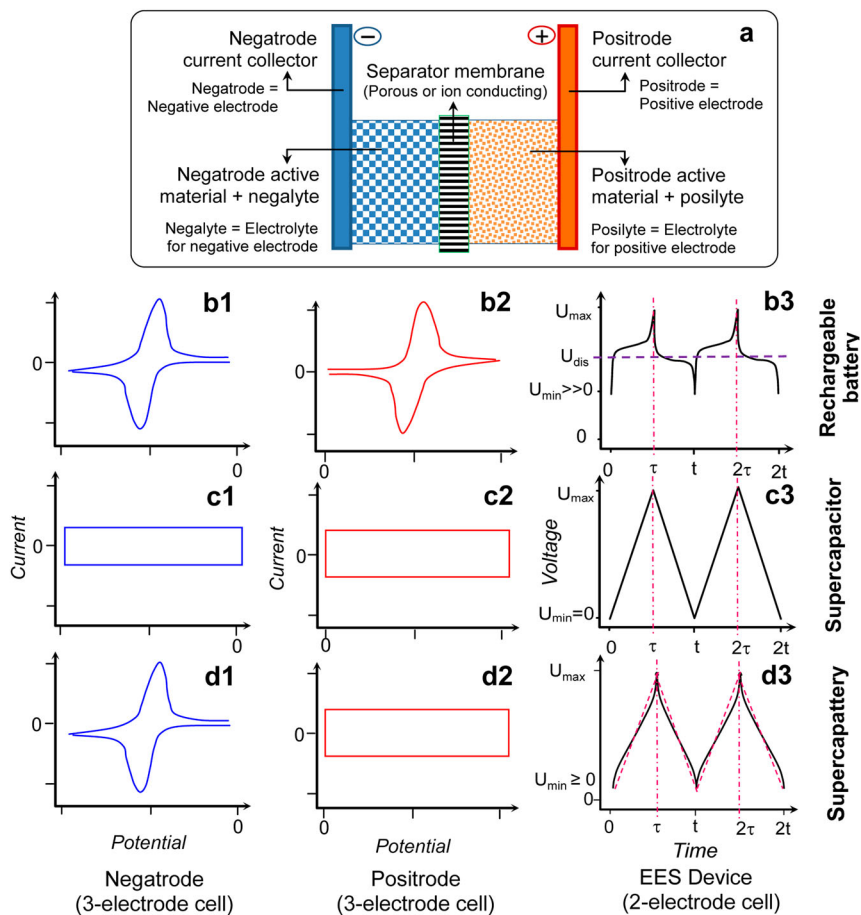


**Figure 2.** Schematic illustrations of (a) a single cell of typical EES devices. (1,2) CVs of positrode and negatode in a three electrode cell, and (3) GCDs of the two electrode cell of (b) rechargeable battery, (c) supercapacitor, or (d) supercapattery.  $U_{\max}$  and  $U_{\min}$ : maximum and minimum cell voltages that can be reached during charging and discharging, respectively, without causing irreversible changes in the cell.  $U_{\text{dis}}$ : average discharging voltage.  $\tau$  and  $t$ : end times of the first charging and discharging cycle,  $\tau \geq (t - \tau)$ .  $2\tau$  and  $2t$ : end times of the second charging and discharging cycle, but not necessarily twice of  $\tau$  and  $t$  [3,5,6].

same Chinese authors often use cathode and anode (which are 阴极 and 阳极 in Chinese) in their English publications [2,17].

There are similar confusions when electrolytes are concerned. In some EES, such as the redox flow battery, the electrolytes are different for the positive electrode

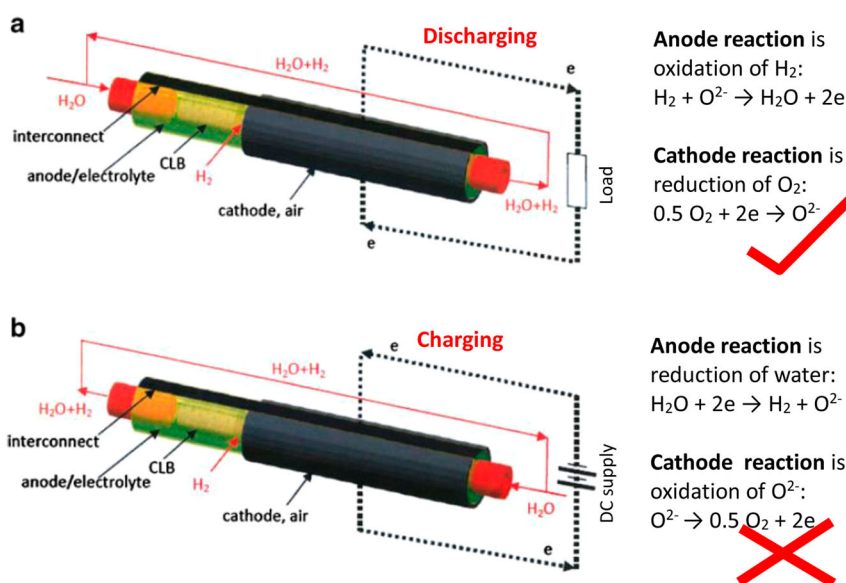


**Figure 3.** Schematic illustration of the solid-oxide redox flow battery (a) the discharge and (b) charge modes. Note the use of the anode and cathode notions can lead to the correct description of the electrode reactions from (a), but the incorrect association of reduction with anode and oxidation with cathode from (b), which is against the definitions of anode and cathode [16]. (Redrawn and reprinted with permission from Springer).

and negative electrode. These are currently called in literature as catholyte and anolyte in line with the cathode and anode notions, which can fall into the same scenario when, for example, oxidation occurs in the catholyte and reduction in the anolyte during charging.

To avoid confusions to newcomers of the EES community and other researchers who are experienced in, for example, materials science but unfamiliar with electrochemical terms, the author proposes positrode and negatrode in places of positive electrode and negative electrode, respectively, as shown in Figure 2(a). Similarly, posilyte and negalyte are proposed for the two separated (e.g. by a membrane) and different electrolytes in contact with the positrode and negatrode, respectively, to avoid confusion with catholyte and anolyte that describe the two separated and different electrolytes in contact with the cathode and anode in an electrolysis cell, respectively. The author also hopes that these one-word terms are convenient to write so that cathode and anode will not be misused for EES. In the following text, these new terms will be used.

In contrast to EDLCs, electrical energy is first converted to chemical energy which is then stored in a rechargeable battery. The chemical reactions are driven by the applied cell voltage and take place on both the positrode and negatrode in the cell, involving electron transfer. Here, electron transfer refers to that between the electrode substrate (or current collector) and the active material on the electrodes in a rechargeable battery, or between the electrode substrate and the redox active ions or molecules in the electrolytes in a redox flow battery. In other words, in the field of EES, electron transfer reactions always refers to those occurring at the boundary connecting two or more phases (solid, liquid and gas). The boundary is an interface between two phases, e.g. 'electrode | electrolyte' and 'current collector | active material', but an interline (or point) between three (or more) phases, such as 'CO | Pt | electrolyte' and 'AgCl | Ag | electrolyte' [18–20]. Such charge transfer reactions are known as Faradaic reactions or processes, so that they are differentiated from those charge transfer reactions, which are often called chemical redox (reduction and oxidation) reactions, between oxidant and reductant molecules occurring in the same liquid solution or at the boundary between two or more phases. The difference is that the transferred electrons in a Faradaic process can be withdrawn from or inject into the electrodes via the external circuit, while in a chemical redox reaction, the electrons are always transferred from the reductant to the oxidant, but not in the reverse direction.

In line with the definition mentioned above, Faradaic reactions are always present and play major roles in energy storage in rechargeable batteries or redox flow batteries, but not in EDLCs. Because of this difference, the minimum voltage for discharging (i.e.  $U_{\min}$  in Figure 2) can decrease to zero in

supercapacitor and supercapattery, but not in rechargeable battery because of possible irreversible changes in the cell when the cell voltage is lower than  $U_{\min}$ .

The link between Faradaic reactions and supercapacitors has been established on the so called pseudocapacitance. This concept was initially associated with the behaviour of adsorbed or deposited monolayer species on electrode in early 1960s [21,22]. Ruthenium dioxide,  $\text{RuO}_2$ , was possibly the first redox active material that was reported in 1971 to be able to exhibit rectangular cyclic voltammograms (CVs) like a capacitor [23]. Similar voltammetric observations were reported for both the ECPs [24–26] and other TMOs [27–30]. However, the early findings of TMOs and ECPs being capable of capacitive storage of charge were not associated with supercapacitors for energy storage until early 1990s [23–25,27]. Because these redox active materials store charge in the capacitive way (i.e. rectangular CVs and linear Galvanostatic charging and discharging plots (GCDs)) that is also Faradaic in nature, but different from that in the EDLC, the concept of pseudocapacitance has also been used.

It is worth mentioning that by convention, a Faradaic process should follow the Nernst equation to produce peak-shaped CVs and non-linear GCDs as shown in Figure 4(a and c), respectively. Such Nernstian behaviour was also observed for the earlier reported electrode reactions of adsorbed species and was attributed to pseudocapacitance [21,22]. For energy or charge storage, the obvious differences between these two types of pseudocapacitance, i.e. rectangular CVs vs. peak-shaped CVs, were long recognised, but the explanation to the differences was based on numerical analysis, instead of a physicochemical attribution [32]. Unfortunately, these important differences have been ignored by quite many authors in recent years. By focusing on the linkage between Faradaic reactions and pseudocapacitance, these authors have applied the concept on some new but battery type materials. As a result, deceptively high specific capacitance values have been claimed, and used in calculation of specific energy [33–36].

The confusion over the concept of pseudocapacitance needs clarification. When it is used to describe the behaviour of adsorbed species and, as a matter of fact, the thin layer coating of a redox active material on the electrode, the current response towards the linear potential change can be expressed as equation (1) below [15]

$$i = \frac{n^2 F^2 A \Gamma_{\text{t}} \nu \exp\left[(E - E^0) \frac{nF}{RT}\right]}{RT \left\{ 1 + \exp\left[(E - E^0) \frac{nF}{RT}\right] \right\}^2} \quad (1)$$

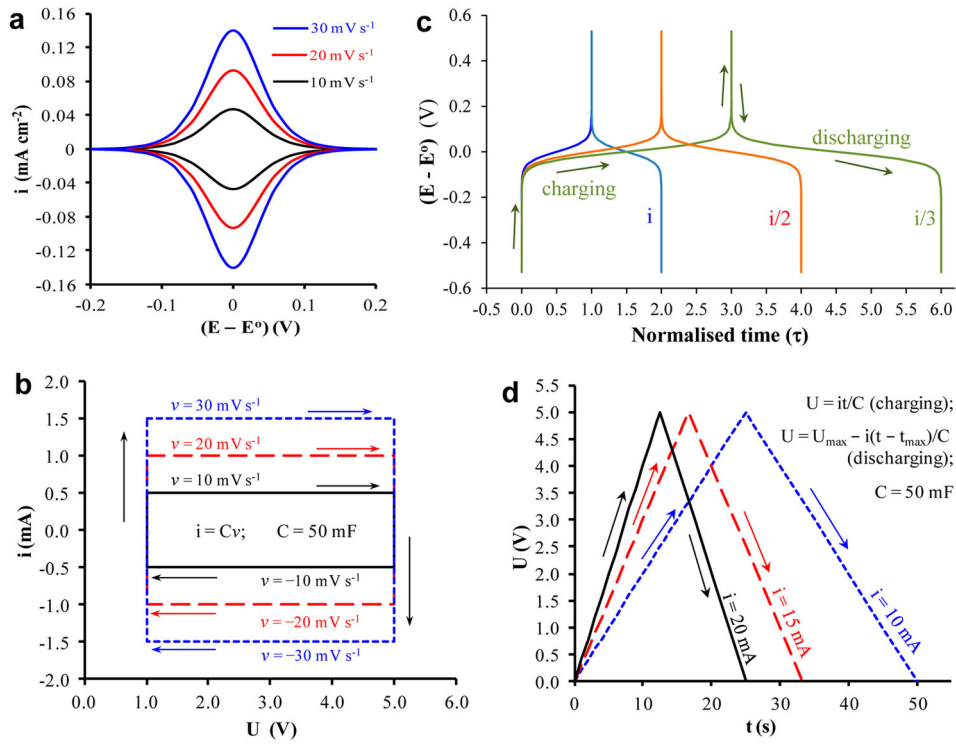


**Figure 4.** (a) CVs derived from equation (1) at indicated potential scan rates, and (c) GCD plots derived from equation (3) at indicated constant currents of  $i, i/2, i/3$  for a reversible Faradaic-Nernstian reaction with localised electron transfer to and from isolated redox sites on the electrode. (b) CVs at indicated voltage scan rates, and (d) GCD plots at indicated constant currents as derived from equation (2) for a capacitor of  $C = 50$  mF with  $U_{\max} = 5$  V. In the GCD plots in (d),  $t_{\max} = U_{\max}C/i$  [3,31].

where  $i$  is the current;  $A$  the geometric area of electrode;  $v$  ( $=dE/dt$ ,  $t$  is the time) the potential scan rate;  $n$  the number of electrons transferred between the reduced and oxidised sites of the adsorbed species;  $\Gamma_t$  ( $=\Gamma_r + \Gamma_o$ ) is the total surface area covered by the reduced ( $\Gamma_r$ ) and oxidised ( $\Gamma_o$ ) sites;  $E$  and  $E^0$  are the applied and equilibrium potentials;  $T$  is the temperature;  $R$ , gas constant ( $=8.314$  J/(mol K<sup>-1</sup>)), and  $F$ , Faraday constant ( $=96485$  C mol<sup>-1</sup>). Assuming  $n = 1$ ,  $A = 1$  cm<sup>2</sup>,  $\Gamma_t = 0.05$ ,  $T = 300$  K, the CVs calculated from equation (1) at three different scan rates are presented in Figure 4(a).

For comparison, the CVs of an ideal capacitor of 50 mF in capacitance are presented in Figure 4(b) as derived from the definition of capacitance, i.e. equation (2),

$$C = \frac{\Delta q}{\Delta U} = \frac{dq/dt}{dU/dt} = i/v \quad (2)$$

where  $q$  is the charge;  $U$  the capacitor (or cell) voltage,  $i$  the current,  $t$  the time, and  $v = dU/dt$  the voltage scan rate. Note that the current polarity is determined by the voltage scan direction (i.e. positive or negative scan), which explains the sharp current switch at both ends of the voltage scan.

The two sets of CVs in Figure 4(a and b) look very different in shape, but they do share two common features, i.e. (1) the proportionality between current and potential or voltage scan rate, and (2) the switch of

current polarity with the scan direction. It was these common features (and other related or derived properties) that had led to the concept of pseudocapacitance in the early literature on adsorption [15,21,22,32]. It should be mentioned that equation (1) describes an equilibrium situation, while slow kinetics of electrode reactions can lead to distortion of the CV shape, mostly the separation of the oxidation and reduction current peak potentials [15,32]. However, the  $i/v$  ratio and also the  $\Delta q/\Delta E$  ratio in Figure 4(a) are a potential or voltage dependent variable, but these ratios remain independent of potential or as a constant in Figure 4(b) and equal to the capacitance,  $C$ .

The GCDs for a capacitor can also be derived from equation (2) as shown in Figure 4(d). For adsorbed species or thin layer coating of a redox active (non-capacitive) material on the electrode, the GCDs, see Figure 4(c), follow equation (3) which is a unique form of the Nernst equation [15].

$$E = E^0 + \frac{RT}{nF} \ln\left(\frac{1-x}{x}\right) \quad (3)$$

where  $x = \Gamma_r/\Gamma_t$  is the mole fraction of reduced species (or sites) on the electrode surface at time  $t$ . Under reversible conditions (i.e. the process is governed by the Nernst equation),  $x$  is linked to the amount of charge passed by Faraday's law as follow.

$$x = \frac{it}{nF\Gamma_t} \quad (4)$$

The obvious differences between Figure 4(c and d) highlight the inappropriateness of using non-linear GCDs for capacitance analysis, and this point is further discussed below.

Similar but less reversible behaviour is commonplace in testing of battery electrode materials. In these cases, the peak potential of oxidation on the CV would shift positively and that of reduction negatively. On the GCD, charging would cause deviation of potential rising upward with time from the plateau, while discharging would decrease the potential downward. Figure 2(b1–b3) depict the expected deviations on CVs and GCDs for a battery and its electrodes. Such behaviour is largely responsible for the relatively low energy efficiency of a battery.

Confusion arises when some authors attempt to use the overall  $\Delta q/\Delta E$  ratio (or the  $\Delta q/\Delta U$  ratio for a two electrode cell) of a peak-shaped CV or a non-linear GCD similar to those in Figures 2 and 3 as the capacitance. Although these authors may not be incorrect to describe their peak-shaped CVs as showing pseudocapacitance in line with the early literature on adsorption [21,22,32] they should have not used the  $\Delta q/\Delta E$  (or  $\Delta q/\Delta U$ ) ratio as capacitance for energy calculation by the following equation [33–36].

$$W = \frac{1}{2} C_{\text{cell}} \Delta U^2 \quad (5)$$

Note that  $C_{\text{cell}}$  in equation (5) is the capacitance of the cell of two electrodes, but not that of a single electrode as in a three or two electrode cell. There are two potential problems. First, energy calculation from a GCD recorded in a two electrode cell is the integration of the plot.

$$W = \int_0^t iUdt = i \int_0^t Udt \quad (6)$$

When  $U$  is a linear function of  $t$ , equation (6) leads to equation (5). In other words, equation (5) cannot be applied for a non-linear GCD. Second, CVs and GCDs are often recorded from a single electrode (in the three electrode cell). In such cases, charge storage can be achieved, which can then be used for calculation of specific charge capacity (peak-shaped CVs and non-linear GCDs) or specific capacitance (rectangular CVs and linear GCDs). However, energy storage and release can only be realised in a two electrode cell, but not from a single electrode. For calculation, the exception is the symmetrical supercapacitor in which the specific capacitance of the electrode material,  $C_{\text{sp}}$ , is simply four-fold of the cell specific capacitance,  $C_{\text{sp,cell}}$ , and can therefore be used for calculation of specific energy,  $W_{\text{sp}}$ . In such cases, the electrode potential window,  $\Delta E$ , measured in the three electrode cell

can be the same as the maximum cell voltage,  $\Delta U$ , measured in the two electrode cell.

$$W_{\text{sp}} = \frac{1}{8} C_{\text{sp}} \Delta E^2 \quad (7)$$

Note that the specific energy,  $W_{\text{sp}}$ , in equation (7) is calculated against the total mass of both the positrode and negatrode. This is different from  $C_{\text{sp}}$  which is calculated against the mass of one electrode. Equation (7) can be used for energy calculation for symmetrical supercapacitors, but not so for an asymmetrical one.

To calculate the specific energy  $W_{\text{sp}}$  of an asymmetrical supercapacitor (or a rechargeable battery), the total mass of both the positrode and negatrode should be used with equation (5) if  $C$  and  $\Delta U$  are measured from the GCD plot of the asymmetrical supercapacitor (not individual electrodes) [or with equation (6) if  $W$  is derived from the GCD of the battery]. For designing an asymmetrical supercapacitor, assuming  $C_{\text{sp+}}$  and  $C_{\text{sp-}}$  to be the specific capacitances,  $m_+$  and  $m_-$  the masses of the positrode and negatrode materials, respectively, the cell specific capacitance,  $C_{\text{sp,cell}}$ , can be calculated as follow.

$$\frac{1}{C_{\text{cell}}} = \frac{1}{m_+ C_{\text{sp+}}} + \frac{1}{m_- C_{\text{sp-}}} \quad (8)$$

$$C_{\text{sp,cell}} = \frac{C_{\text{cell}}}{m_+ + m_-} \quad (9)$$

$C_{\text{sp,cell}}$  from equation (9) can be used to replace  $C_{\text{cell}}$  in equation (5) to calculate  $W_{\text{sp}}$ , instead of  $W$ .

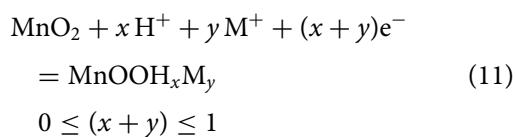
## Mechanisms of charge transfer and storage in materials

Reversible storage (charging) and release (discharging) of electric charge is the basis for all successful EES devices, although the charging–discharging mechanisms differ significantly, depending on where and how the charge is stored. EDL storage occurs at the interface between the electrode and electrolyte and is two dimensional in nature. It may be argued that when the electrode is sufficiently porous and contains a significant portion of well distributed micro-pores, EDL storage also becomes three dimensional. However, when inspected at molecular scale, EDL storage still remains two dimensional. In contrast, Faradaic storage proceeds inside the material and is intrinsically three dimensional at both macroscopic and molecular scales, giving rise to significantly higher specific charge capacity ( $\text{mAh g}^{-1}$ ) or specific capacitance ( $\text{F/g}$ ) compared with EDL storage. Figure 5 illustrates schematically the charge storage mechanisms in (a) a carbon powder electrode via EDL capacitance and (b) a conducting polymer electrode via pseudocapacitance. The definition equation of capacitance,  $C = \epsilon_0 \epsilon A/d$ , is shown inside the enlarged carbon particle in Figure 5

(a) with  $A$  being the interfacial area,  $d$  the thickness of the EDL,  $\epsilon$  the dielectric constant (or relative permittivity), and  $\epsilon_0$  the vacuum permittivity ( $=8.854 \times 10^{-12}$  F/m). In Figure 5(b), charge storage is achieved via pseudocapacitance, i.e. the electro-oxidation of polyaniline that generates positive charges along individual polymer chains. Counter anions ( $A^- = \text{Cl}^-, \text{HSO}_4^-, \text{etc.}$ ) are driven into the polymer structure by the electrode potential to maintain electric neutrality. It should be pointed out that the situation depicted in Figure 5(b) can actually be applied to the Faradaic processes in battery electrode materials to a certain degree. Some clarifications are thus needed and given below.

Faradaic processes can offer either capacitive or non-capacitive behaviour, but both involve electron transfer processes (or redox reactions). Non-capacitive Faradaic processes are governed broadly by the Nernst equation and hence can also be called Nernstian processes. On performance, Nernstian processes are featured by peak-shaped CVs and non-linear GCDs with one or more potential plateaux. These features are fundamentally related to the fact that the electron transfer reaction in a Nernstian process occurs when the electrode potential reaches at and beyond the unique equilibrium potential,  $E^0$ , which is a constant for a given reaction at the working temperature. For a capacitive Faradaic process which is the basis of pseudocapacitance in the context of supercapacitors, rectangular CVs and linear GCDs are the common features which cannot be explained simply or easily by the Nernst equation. Note that there were many claims of high values of specific pseudocapacitance derived from peak-shaped CVs or non-linear GCDs [33–36] but these are misleading and excluded from discussion here because of reasons as discussed above and highlighted in both earlier and recent literature [3,5,32,40,41].

It has been proposed that the rectangular CV of a TMO based pseudocapacitive material is the result of ‘multiple surface successive redox reactions’ which involves sub-stoichiometric variation in the electrode material and electro-adsorption of proton or cations. These reactions can be described below similarly for ruthenium oxides, Ru (IV-II), and manganese oxides Mn (IV-III) [42].



Note that the chemical formulae in both (10) and (11) can be written in other forms such as  $\text{RuO}_{2-x}\text{H}_x\text{O}$ ,  $\text{RuO}_{2-x}(\text{OH})_x$  and  $\text{Li}_z\text{MnO}_x(\text{OH})_y$  which are more complex, but do emphasise the hydrous nature of these oxides [42–44]. There are other TMOs that can

offer capacitive Faradaic charge storage reactions similar to reactions (10) and (11), such as  $\text{V}_2\text{O}_5$ ,  $\text{SnO}_2$  and  $\text{Fe}_2\text{O}_3$  [36,40,45]. The proposal of ‘multiple surface successive redox reactions’ however needs to answer some further questions. For example, why do these reactions only occur at the surface, and why do they not proceed with one full electron and one full cation?

In fact, in addition to TMOs, ECPs, such as polypyrrole (PPy), polyaniline (PAN) and poly 3,4-ethylenedioxythiophene (PEDOT), can also exhibit capacitive Faradaic behaviour [24–27,39,46]. It should be mentioned that activated carbon retains capacitive performance, i.e. the rectangular CVs, over the whole potential window of the aqueous electrolyte. This is exemplified in Figure 5(c) by the CVs recorded in different potential ranges [38]. It can be seen that when the potential range is gradually extended, a reduction reaction (cathodic or negatropic reaction as labelled in Figure 5(c)) appears at  $-1.1$  V vs. Ag/AgCl. This reaction corresponds to  $\text{H}^+ + \text{e}^- = \text{H}_{\text{ad}}$ , and the produced  $\text{H}_{\text{ad}}$  in the micro-pores of the activated carbon is re-oxidised when the potential is scanned back to around 0.5 V which is evident by the small re-oxidation peak. Beyond this small re-oxidation peak, a further oxidation current (anodic or positropic reaction) appears at potentials beyond 0.8 V. This is likely due to oxidation of water,  $2\text{H}_2\text{O} = \text{O}_2 + 4\text{H}^+ + 4\text{e}^-$ , and/or oxidation of carbon,  $\text{C} + 2\text{H}_2\text{O} = \text{CO}_2 + 4\text{H}^+ + 4\text{e}^-$ . Between these two limits, the activated carbon exhibited satisfactory capacitive currents on both the positive and negative potential scans.

In Figure 5(d), however, the CVs show that polyaniline only exhibits capacitive performance in a limited potential range between 0.1 and 0.8 V [39]. Widening the potential range leads to current peaks near both the positive and negative ends of the potential scan. Similar behaviour has been observed for PPy and PEDOT [47]. Because ECPs become insulating when they are reduced, the current peaks at less positive potentials are known to be linked with the oxidation induced doping (by anions) and reduction induced de-doping. Doping and de-doping of the polymer is accompanied by the conversion between the insulating and conducting phases of the polymer. For polyaniline, the current peaks at more positive potentials are due to formation of other forms of the polymer which are also less conducting [39,47]. For PPy, PAN and PEDOT, the rectangular CVs can be achieved by maintaining the polymer in the doped and partially doped states, i.e. in the potential range where complete reduction of the polymer is avoided. In other words, as long as the polymer remains sufficiently conducting, it will behave in the capacitive way.

Interestingly, although both  $\text{RuO}_2$  and  $\text{MnO}_2$  are widely studied for their pseudocapacitance, changing experimental conditions can also cause current peaks appearing on their CVs [48–50]. Figure 6 compares

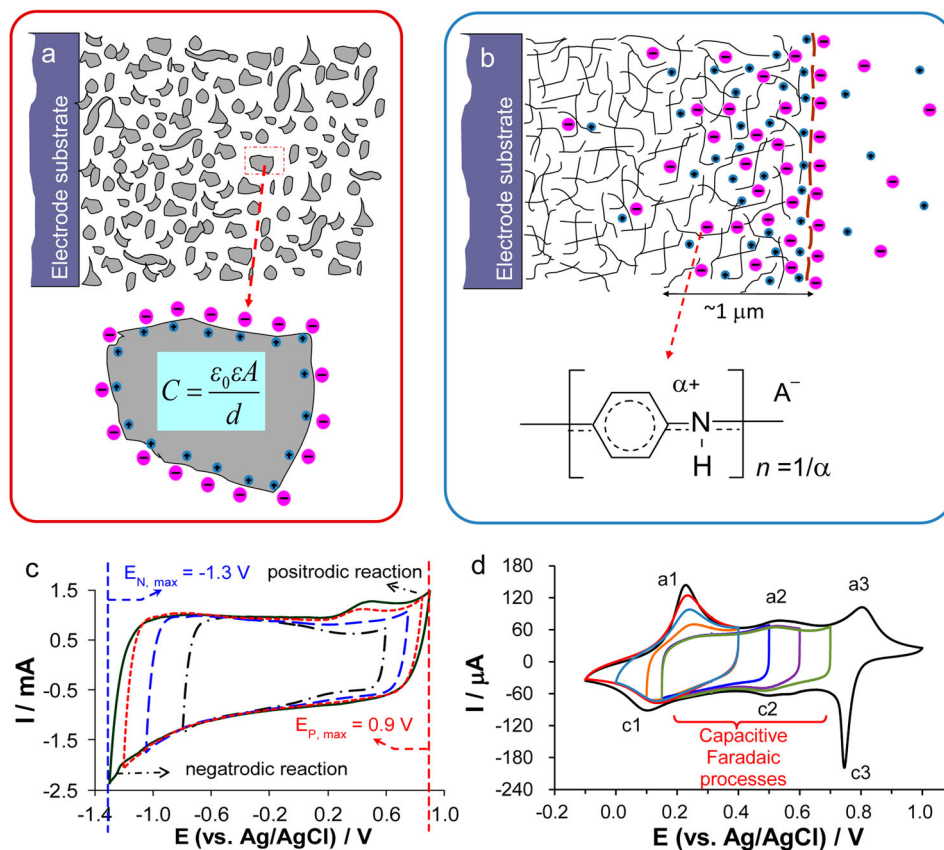


**Figure 5.** (a, b) Schematic views of the cross-sections of (a) a carbon powder electrode and (b) a polyaniline electrode. The enlarge view below (a) shows charge storage on a single carbon particle via ion adsorption at the carbon | electrolyte interface, i.e. the EDL capacitance [37]. (c, d) CVs of (c) activated carbon [38] (2.5 mg) in  $0.3 \text{ mol L}^{-1} \text{ K}_2\text{SO}_4$  at  $5 \text{ mV s}^{-1}$  and (d) electrodeposited polyaniline [39] (10 mC) in  $1.0 \text{ mol L}^{-1} \text{ HCl}$  at  $20 \text{ mV s}^{-1}$  in different potential ranges.

the CVs recorded in two different potential ranges on a graphite disc electrode whose surface contained trenches in which was filled the powder of the composite of  $\text{MnO}_2$  and CNTs [50]. The CVs recorded in the wider potential range ( $-0.8$ – $0.9 \text{ V}$  vs. Ag/AgCl) show a clearer couple of current peaks, see Figure 6(a), which can be attributed to the redox couple of Mn (III/II) and responsible for the fairly fast decay of the current on the CVs during only 100 potential cycles [50,51]. However, by positively shifting the negative potential end to avoid the reduction to the Mn (II) state which is soluble in aqueous solution [51] the CV becomes more rectangular and stable as shown in Figure 6(b).

The influence of potential range on the CV shape as shown in Figure 5(d) and Figure 6 suggests that the origin of pseudocapacitance is likely related with a unique state of the material in terms of doping level, valence and/or conductivity. In this state, there is not a fixed equilibrium potential for the Faradaic (or electron transfer) reaction, but the potential has a continuous and constant influence in a noticeable potential range. Such capacitive behaviour cannot be explained by the Nernst equation, but it follows well with the semiconductor band model as explained in more details below.

When prepared in an appropriate form, both TMOs and ECPs can possess semi-conductivity which can be explained in relation with energy level of valence

electrons in the material by the band model for chemical bonding as illustrated in Figure 7 [32,52]. Using metals as an example, the evolution of energy levels is presented from that of individual and separated atoms to that in clusters of 2, 5, 20 and  $10^{20}$  atoms.

On the left side of Figure 7 is shown the energy levels of two orbits for non-interactive atoms (or atomic ions). The orbit of lower energy is filled with valence electrons, and the higher energy orbit is empty. Such valence electrons are fixed at a unique energy level, and hence referred as localised valence electrons. When two atoms are bonded, the original orbits of the atoms are split into more sub-orbits of different energy levels, and the number of sub-orbits depends on if the valence electrons are on the s, p, d or f orbitals. Because the number of valence electrons remains the same before and after bonding, some of the sub-orbits at lower energy levels will be occupied, but the others are vacant.

Bonding more atoms into a cluster increases the number of sub-orbits in a multiple manner, while the gap between neighbouring energy levels of sub-orbits becomes smaller. Again, all the valence electrons occupy the sub-orbits at lower energy levels, leaving other sub-orbits unoccupied at higher energy levels. The sub-orbits are separated into two groups by a unique energy gap,  $E_g$ , between the lowest energy

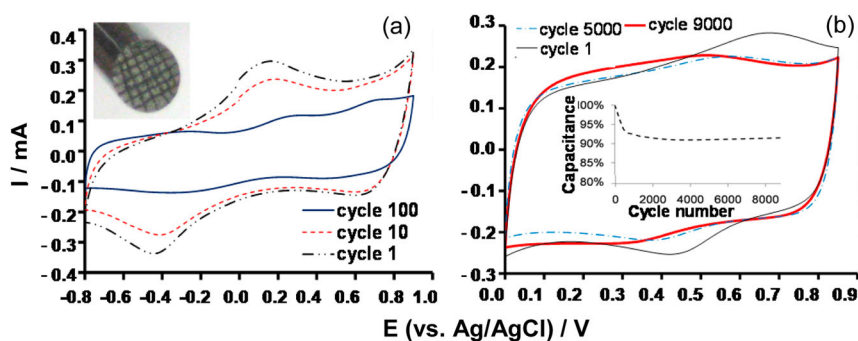


**Figure 6.** CVs of  $\text{MnO}_x/\text{CNTs}$  composites in  $0.5 \text{ mol L}^{-1}$  KCl at  $10 \text{ mV s}^{-1}$  recorded during continuous potential cycling in the potential ranges of (a)  $-0.80$  to  $0.90 \text{ V}$  (Inset: photo of a trenced graphite disk electrode) and (b)  $0.0$ – $0.85 \text{ V}$  (Inset: plot of the relative capacitance against the number of potential cycles) [50].

level of the higher energy group, and the highest energy level of the lower energy group. By further increasing the number of atoms in bonding, the difference between neighbouring energy levels within the same group becomes so small that the energy change becomes continuous to form an energy band. The higher energy group is known as the conduction band (CB), but it is vacant in absence of any external effect (e.g. light). The lower energy group is given the name of valance band (VB). In most cases, the VB is partially occupied by valence electrons because the original atomic orbits are not fully occupied by valence electrons. As a result, valence electrons are able to move between the occupied and unoccupied orbits easily within the VB, offering different levels of semi-conductivity. In other words, the valence electrons

are delocalised in the VB. Obviously, when more atoms are added in the cluster, the number of energy levels and also the degree or zone size of delocalisation increase, but the gap between neighbouring energy levels decreases. Eventually, the number of atoms in the cluster is so large (e.g.  $10^{20}$ ) that the VB and CB are merged, leading to complete delocalisation of the valence electrons and fully metallic conductivity. Note that the drawing in Figure 7(b) is actually equally applicable to other semiconductor materials in which delocalisation of valence electrons occurs to different degrees and zone sizes, depending on, for example, the crystallinity of the material. Also, delocalisation can be either one, two or three dimensional as in the individual chains of polypyrrole, graphene or manganese dioxide, respectively.

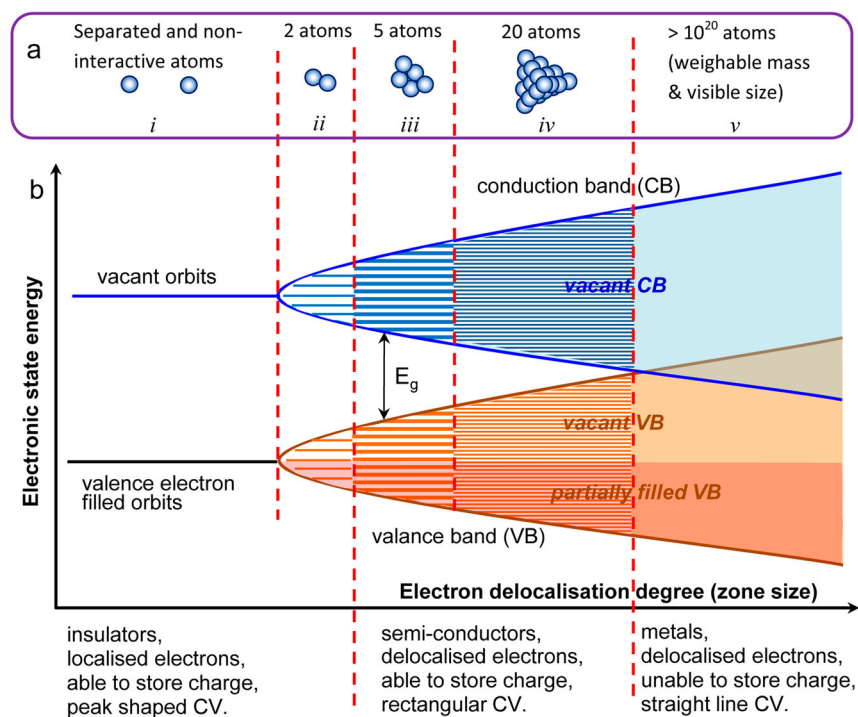


**Figure 7.** Schematic illustrations of the band model for chemical bonding [15] (a) between metal atoms that are (i) separated and non-interactive, and (ii – v) forming clusters of (ii) 2, (iii) 5, (iv) 20 and (v)  $10^{20}$  atoms, [52] and (b) the corresponding energy levels of the valence electrons as a function of the degree (or zone size) of delocalisation of valence electrons in the cluster of metal atoms [15].

In line with the band model, the Nernstian behaviour corresponds to electron transfer to or from isolated redox centres, such as those in a solid insulator or liquid electrolyte, where the valence electrons are localised. In other words, all the electrons transferred will enter or leave the orbits of the same energy level (of different redox centres) as shown on the far left side of Figure 7. This in turn means that the Faradaic reaction proceeds at potentials of a narrow range around the equilibrium potential,  $E^\circ$ , and hence the current peaks on CV, or the potential plateau on GCD.

In the semiconductor region, there are many more orbits of very close energy levels over a wide range or a band. Thus, the potentials at which electron transfer take place also range widely but very close to each other, i.e. every small change in potential can cause an electron transfer, leading to a constant current flow in the capacitive way with a linearly varying potential, or a linearly varying potential under a constant current. This capacitive Faradaic process is the origin of the pseudocapacitance in the context of supercapacitors, which was however not recognised until recently [3,31,37].

An important nature of the band model is that each electron is transferred to a particular energy level that is shared by many atoms. Consequently, there is no longer a fixed stoichiometry between the number of electrons transferred and the number of atoms involved. In other words, the reaction stoichiometry becomes fractional as exemplified by reactions (10) and (11). Such fractional stoichiometry makes it challenging to derive the theoretical specific charge capacity and hence specific capacitance if the potential range is given, for pseudocapacitive materials.

One may argue that an integer number of electrons transferred in reactions (10) or (11) can be used for calculation of the theoretical specific charge capacity. However, caution must be applied when deriving specific capacitance because in the potential range for a full electron transfer per atom, the electrode reaction may cause a peak-shaped CV which invalidates capacitive analysis. Figure 8(a) shows clearly the peak-shaped CV of the composite of Ni(OH)<sub>2</sub> and graphene in concentrated aqueous KOH solution in a potential range of 0–0.55 V [34]. Non-linear GCDs were also recorded from this material as shown in Figure 8(b). Based on these data, it can be confirmed that the specific charge capacity of the composite is close to the theoretical value of  $Q_{sp} = nF/M_{Ni(OH)_2} = 1040.94 \text{ C/g}$  (289.15 mAh g<sup>-1</sup>) for the one-electron oxidation of Ni(OH)<sub>2</sub>. However, the specific charge capacity data were brought into equation (2) ( $C = \Delta q/\Delta E$ ) to claim high specific capacitance values (1335 F/g and 935 F/g against the mass of Ni(OH)<sub>2</sub> only and of total sample, respectively, at 2.8 A/g). Surprisingly and incorrectly, such obtained specific capacitance values were brought into equation (5),

instead of equation (7), to derive meaningless ‘energy density’ values (37–53 Wh kg<sup>-1</sup>). Here, energy density is mistaken for specific energy). The worse scenario appears when this Ni(OH)<sub>2</sub>-graphene composite is considered for making a symmetrical supercapacitor as explained below.

Apparently, a careful look at the CV in Figure 8(a) reveals that to make a symmetrical supercapacitor using this Ni(OH)<sub>2</sub>-graphene composite, the cell voltage would be the same as the potential range of the CV. Further, the potential ranges of the positrode and negatrode should be those marked as  $\Delta E_P$  and  $\Delta E_N$ , respectively, in Figure 8(a). However, the CV shows that in  $\Delta E_P$  oxidation can occur, but there is little reduction, and in  $\Delta E_N$  reduction can occur but no oxidation is possible. This means that a symmetrical supercapacitor of this composite would not be charged or discharged. This conclusion can also be derived from the GCD in Figure 8(b). For a true capacitive material with a specific capacitance of 1335 F/g in the potential range of 0.55 V, the GCDs of the positrode ( $E_P$ ) and negatrode ( $E_N$ ), and the symmetrical cell ( $U_{cell} = E_P - E_N$ ) would look like those shown in Figure 8(c). Using the plot in Figure 8(b), the GCD of the positrode and negatrode and the symmetrical cell can be derived as shown in Figure 8(d). Clearly, the  $U_{cell}$  curve in Figure 8(d) shows a charging process but no discharging, which agrees with the above analysis of the CV.

Because their charge storage and release processes are reversible, all capacitive materials can be applied in symmetrical supercapacitors. Thus, the Ni(OH)<sub>2</sub>-graphene composite discussed above is obviously not a capacitive material in a relatively wide potential range (>0.5 V). On the other hand, this nanostructured composite did show good charging–discharging rates and very stable behaviour in over 2000 charging–discharging cycles. Similar properties were reported for other nanostructured composite materials that exhibit peak-shaped CVs and non-linear GCDs. These non-capacitive faradaic properties make it worthwhile to pair such a composite with a capacitive material in a supercapattery. It should be emphasised that if a non-capacitive faradaic material undergoes reversible charging and discharging, i.e. the CV looks like that in Figure 4(a), it can also be made into a symmetrical device, although the cell voltage may be relatively small. More discussion will be given later in this article.

It must be highlighted that the capacitive Faradaic charge transfer (storage or release) in all known materials can only occur in a limited range of potentials, although this range could be wider than 1.0 V. This capacitive potential range is an intrinsic and characteristic property of the material, but it is also significantly affected by the electrolyte used. For example, MnO<sub>2</sub> exhibits pseudocapacitance in a fairly wide potential range, –0.10 to 0.85 V vs. Ag/AgCl, in a

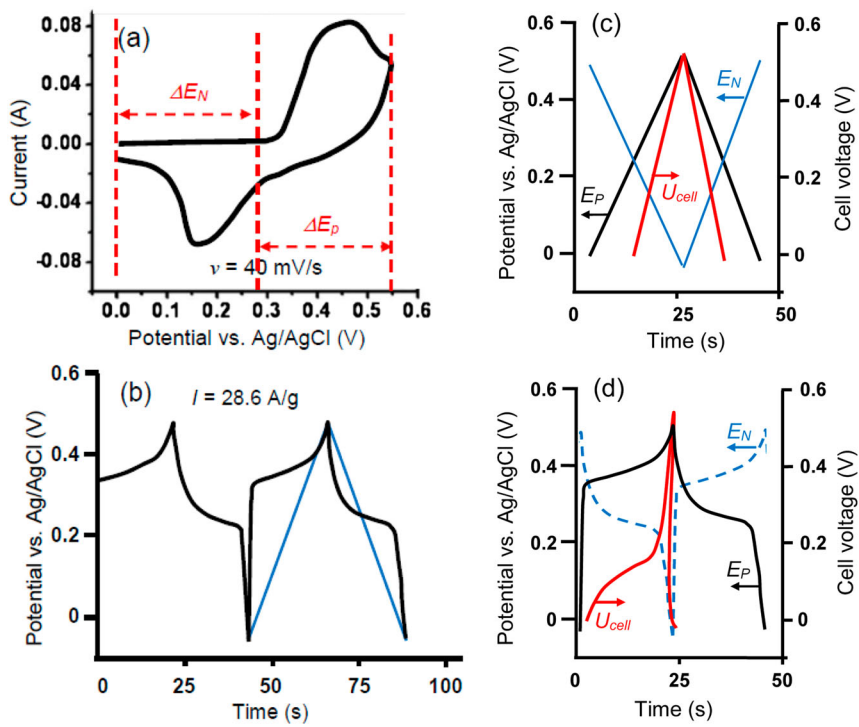


**Figure 8.** (a) Peak-shaped CV and (b) non-linear GCD of nanoparticles of  $\text{Ni}(\text{OH})_2$  grown on graphene sheets in a  $6 \text{ mol L}^{-1}$  KOH aqueous electrolyte (redrawn from Wang et al. [34]). The blue line superimposed in (b) represents the GCD of an ideal capacitive electrode with the same  $\Delta Q/\Delta E$  ratio ( $\Delta Q$ : charge = current  $\times$  time;  $\Delta E$ : potential difference) as that of the non-linear GCD of the  $\text{Ni}(\text{OH})_2$ -graphene composite (black line). (c) and (d) show the GCDs of hypothetical symmetrical cells (red line,  $U_{\text{cell}} = E_p - E_n$ ) constructed respectively using the same (c) capacitive material and (d)  $\text{Ni}(\text{OH})_2$ -graphene composite as the positrode (black line,  $E_p$ ) and negatrode (blue dashed line,  $E_n$ ).

neutral aqueous electrolyte, e.g. KCl. However, the material behaves more like a battery electrode material when the negative end of potential scan is extended to a more negative potential, e.g.  $-0.8 \text{ V}$  as shown in Figure 6(a) [50]. In fact,  $\text{MnO}_2$  has been long studied in alkaline electrolytes and peak-shaped CVs were obtained in relatively wide potential windows, e.g.  $-1.1$  to  $0.5 \text{ V}$  vs.  $\text{Hg}/\text{HgO}$  [53]. In a narrower potential window from  $-0.3$  to  $0.6 \text{ V}$  vs.  $\text{Hg}/\text{HgO}$ , fairly rectangular CVs were also obtained [54]. Another example is  $\text{NiO}$  (or  $\text{Ni}(\text{OH})_2$ ) which is also a long studied electrode material for charge storage [55,56]. A strong couple of current peaks appear on the CVs in the potential range of  $-0.3$  to  $0.8 \text{ V}$  vs.  $\text{Hg}/\text{HgO}$  in concentrated KOH solutions (cf. Figure 8(a)) [55]. Similar observations were reported in more dilute KOH (3 wt-%), but the CV became almost ideally rectangular when the potential range was narrowed to  $0$ – $0.35 \text{ V}$  vs. SCE [56]. In this narrow potential window, the specific capacitance of  $\text{NiO}$  as derived from the rectangular CVs could be over  $100 \text{ F/g}$ . This finding is in contrast with a recent comment that  $\text{NiO}$  is not a pseudocapacitive material by nature [40].

On the other hand, as discussed above, in the potential window where peak-shaped CVs are observed,  $\text{Ni}(\text{OH})_2$  (or  $\text{NiO}$  and similarly nanostructured materials) can exhibit satisfactorily high specific charge capacity and also very stable charge–discharge cycling behaviour. Thus, such nanostructured materials are still

good candidates for EES devices, such as supercapattery and supercabattery. They should just not be chased as capacitive or pseudocapacitive materials, and all their previously reported high specific capacitance values based on peak-shaped CVs and/or non-linear GCDs should be disregarded.

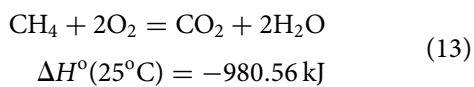
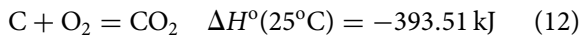
In the region of complete delocalisation of valence electrons as in metals, charge storage is not possible because the electrons will flow freely to the surface or out of the material even when a small polarisation is applied. As a result, metals can only offer limited capacitive charge storage via the EDLC mechanism. However, because it is difficult to prepare metallic samples with high specific area in comparison with activated porous carbon and other porous materials with nanostructures, metals are mostly used as the electrode substrate (current collector). Nevertheless, porous metals, such as the widely used nickel foam, can still be useful in fabrication of EES devices, functioning as excellent electrode substrate for loading of powdery active materials.

In summary, electrochemical charge (and energy) storage can proceed in three different mechanisms, i.e. EDLC, capacitive faradaic processes (pseudocapacitance), and non-capacitive faradaic processes (Nernstian behaviour). Of these three mechanisms, the concept of EDL as shown in Figure 1(a), and the Nernst equation (3) are well described in classic textbooks of electrochemistry. Although pseudocapacitance was

initially proposed to account for some adsorption phenomena, its definition and meaning in the context of supercapacitor have evolved to an emphasis of the capacitive nature against the commonly observed Nernstian behaviour of many adsorbents on electrode.

### Rechargeable battery vs. supercapacitor and their hybrid: supercapattery

In their early development and commercial production, EES devices, particularly rechargeable batteries, have been used predominantly as the power source in various portable devices. These include lighting in dark and remote areas, electrical and electronic appliances, and ignition for internal combustion engines. Power supply as backup for short period, and for vehicles travelling in short distances are also common, while large scale and long duration energy needs are mainly based on fossil fuels, which are now expected to be replaced at least to a significant part by renewables. This development is inevitable and greatly needed, but it faces a primary challenge in terms of specific energy ( $\text{Wh kg}^{-1}$ ) or energy density ( $\text{Wh L}^{-1}$ ). Fossil fuels typically contain 10–20 kWh  $\text{kg}^{-1}$  in specific energy as can be derived from enthalpy changes of the following two combustion reactions with carbon (coal) and methane (natural gas) as examples. Note that the room temperature of 25°C is applied in calculation of the enthalpy change,  $\Delta H^\circ$ , so that the values can be compared with those discussed later for battery reactions.



The specific enthalpy,  $\Delta H_{\text{sp}}^\circ$ , of carbon and methane combustion in  $\text{Wh kg}^{-1}$  can be derived by the following equation,

$$\Delta H_{\text{sp}}^\circ = \frac{\Delta H^\circ}{\sum \gamma_{r,j} M_{r,j}} = \frac{\Delta H^\circ}{\sum \gamma_{p,j} M_{p,j}} \quad (14)$$

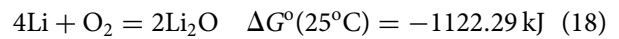
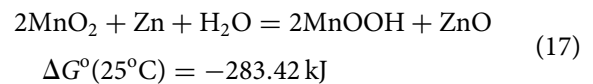
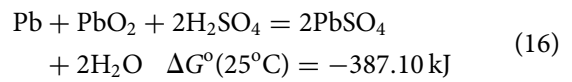
where  $M_{p,j}$  and  $M_{r,j}$  represent the formula masses, and  $\gamma_{r,j}$  and  $\gamma_{p,j}$  are stoichiometric coefficients of the  $j$ th reactant and product, respectively. Since 1 Wh = 3600 J, the calculated specific enthalpy values are  $-2.48$  and  $-3.41$  kWh  $\text{kg}^{-1}$  for carbon and methane, respectively. However, because  $\text{O}_2$  is a gas and can be obtained from air, it is practically reasonable to ignore the  $\text{O}_2$  mass in the calculation, leading to  $-9.11$  and  $-17.06$  kWh  $\text{kg}^{-1}$  for carbon and methane, respectively. The enthalpy change can be directly linked to the heat that is needed for warming a house, for example. However, for the power needed to drive a car, for instance, not all the enthalpy change can be converted to work because of the entropy loss. The

portion of the enthalpy change available for doing work is the Gibbs free energy change,  $\Delta G^\circ$ , which is linked to the enthalpy and entropy changes,  $\Delta S^\circ$ , by the following equation.

$$\Delta G = \Delta H - T\Delta S \quad (15)$$

The specific Gibbs free energy changes of reactions (12) and (13) can then be calculated, taking into account only the mass of the fuel, to be  $-9.13$  and  $-14.20$  kWh  $\text{kg}^{-1}$ , respectively. Note that the entropy change is positive for reaction (12) but negative for (13).

Similar calculations can be applied to battery reactions, but in such cases, it is the Gibbs free energy change, i.e.  $\Delta G^\circ$ , that matters. For the classic lead-acid battery and alkaline zinc-manganese dioxide battery, and the more advanced lithium-air battery, the cell reactions are as follow.



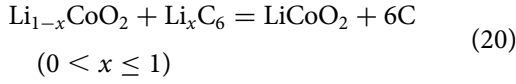
Similar to equation (14), specific Gibbs free energy,  $\Delta G_{\text{sp}}^\circ$ , can be expressed as

$$\Delta G_{\text{sp}}^\circ = \frac{\Delta G^\circ}{\sum \gamma_{r,j} M_{r,j}} = \frac{\Delta G^\circ}{\sum \gamma_{p,j} M_{p,j}} \quad (19)$$

Thus, for the lead-acid battery,  $\Delta G_{\text{sp}}^\circ = -167.34$  Wh  $\text{kg}^{-1}$  and for the alkaline Zn-MnO<sub>2</sub> battery  $\Delta G_{\text{sp}}^\circ = -306.10$  Wh  $\text{kg}^{-1}$ . In reality, due to mainly kinetic causes, the specific energy of the lead-acid battery is only 30–40 Wh  $\text{kg}^{-1}$ , while that of the alkaline Zn-MnO<sub>2</sub> battery reaches 90–150 Wh  $\text{kg}^{-1}$  [57,58]. Although the Li-O<sub>2</sub> battery via reaction (18) can reach a very high value of  $\Delta G_{\text{sp}}^\circ = -5216.48$  Wh  $\text{kg}^{-1}$ , this new device still remains in research and development due to various challenges such as fundamental understanding, materials stability and device engineering [59]. Note that for the Li-O<sub>2</sub> battery, because  $\text{O}_2$  is supplied from air, it is tempting to ignore the mass of  $\text{O}_2$  in calculation of the specific energy so that  $\Delta G_{\text{sp}}^\circ = -11228.47$  Wh  $\text{kg}^{-1}$  [60]. However, this is inappropriate because the discharging produced  $\text{Li}_2\text{O}$  would remain in the battery.

Not all battery reactions can be found in available thermodynamic databases, but it is still possible to derive their  $\Delta G_{\text{sp}}^\circ$  values from the battery's discharging performance. For example, for the commercialised lithium ion battery, the following reaction can be established with graphite anode and lithium cobalt oxide

positrode,



where  $x = 1$  or  $0$  corresponds to a fully charged or discharged state of the battery, involving the transfer of 1  $\text{Li}^+$  ion and 1 electron. Thus, the theoretical specific discharging capacity,  $Q_{\text{sp,cell}}$ , for the cell reaction can be calculated to be  $157.77 \text{ mAh g}^{-1}$  according to the equation below with  $n = 1$ .

$$Q_{\text{sp,cell}} = \frac{nF}{\sum \gamma_{r,j} M_{r,j}} = \frac{nF}{\sum \gamma_{p,j} M_{p,j}} \quad (21)$$

It is well established that the discharging cell voltage is  $3.5 \text{ V}$  on average for this lithium ion battery, which in turns gives rise to  $552.2 \text{ Wh kg}^{-1}$  in the cell specific energy. Note that the cell voltage can be linked to  $\Delta G^\circ$  by equation (22) below.

$$\Delta G^\circ = -nFU_{\text{cell}} \quad (22)$$

For  $n = 1$ , combining equations (22) and (19) can also lead to  $\Delta G_{\text{sp}}^\circ = 552.2 \text{ Wh kg}^{-1}$ . It should be mentioned that in the literature, the specific charge of an electrode material,  $Q_{\text{sp}}$ , is often reported. Theoretically,  $Q_{\text{sp}} = nF/M$  where  $M$  is the formula mass, and it can be calculated to be  $1340 \text{ C/g}$  or  $372 \text{ mAh g}^{-1}$  for carbon, and  $1061 \text{ C/g}$  or  $295 \text{ mAh g}^{-1}$  for  $\text{CoO}_2$  according to reaction (20).

For supercapacitors, calculation of the theoretical specific energy of the cell needs to be carried out according to the charge storage mechanism. For a symmetrical EDLC, charge storage involves no chemical reaction in theory. Thus, the cell specific energy is then directly derived from the maximum cell voltage,  $U_{\text{cell}}$ , which is usually the decomposition voltage of the electrolyte used, and the specific capacitance,  $C_{\text{sp}}$ , of the electrode material according to equation (7). The value of  $C_{\text{sp}}$  is in principle the product of the double layer capacitance,  $C_{\text{d}}$  (cf. Figure 1(a)), and the specific area,  $A_{\text{sp}}$ , of the material in contact with the electrolyte used, i.e.

$$C_{\text{sp}} = C_{\text{d}}A_{\text{sp}} \quad (23)$$

$C_{\text{d}}$  is also known by another name, the differential capacitance [15]. Note that  $C_{\text{d}}$  may change with potential in dilute electrolytes at potentials near the so called 'potential of zero charge' (PZC) [15]. However,  $C_{\text{d}}$  becomes potential independent at high electrolyte concentrations (e.g.  $\geq 1 \text{ mol L}^{-1}$ ) [15] which is always true in supercapacitors. The value of  $C_{\text{d}}$  is typically in the range from  $10$  to  $40 \mu\text{F cm}^{-2}$  as measured on a flat macro-electrode made from many metallic and carbon materials in aqueous electrolytes. Thus, in theory, for a porous and powdery material with a specific area of  $1000 \text{ m}^2 \text{ g}^{-1}$ , the specific capacitance resulting solely from double layer capacitance can range from  $100$  to

$400 \text{ F/g}$ . It means a value of specific energy,  $W_{\text{sp}}$ , ranging from  $7.81$  to  $31.25 \text{ Wh kg}^{-1}$  for a symmetrical supercapacitor containing a neutral aqueous electrolyte with a cell voltage of  $1.5 \text{ V}$  according to equation (7). In organic electrolytes, the cell voltage is higher than  $2.5 \text{ V}$ , although the  $C_{\text{d}}$  value is smaller than in aqueous electrolytes. Because  $W_{\text{sp}}$  is proportional to squared cell voltage, organic electrolyte based supercapacitors offer higher  $W_{\text{sp}}$  values than the aqueous ones. In reality, the highest  $C_{\text{sp}}$  value for EDL materials based on undoped or unmodified activated carbons and graphenes is about  $200 \text{ F/g}$  which is well in line with the specific area of the material according to equation (23). However, upon modification or doping, higher  $C_{\text{sp}}$  values have been reported for materials with low  $A_{\text{sp}}$  values, which have been generally attributed to the modification or doping induced redox activity into the materials which contributed to pseudocapacitance [60,61].

Interestingly, a recent study has claimed that in nitrogen doped carbon prepared from pyrolysis of nitrogen rich polymers, there are abundant 'ultramicro-pores' ( $<0.5 \text{ nm}$ ) that are not detectable by the  $\text{N}_2$  adsorption, but can be accessed by  $\text{CO}_2$  and small ions (e.g.  $\text{K}^+$  and  $\text{OH}^-$ ). Consequently, the measured  $C_{\text{sp}} = 151 \text{ F/g}$  was claimed to be still EDLC in nature because the specific surface area measured from  $\text{N}_2$  adsorption ( $A_{\text{sp}} = 60 \text{ m}^2 \text{ g}^{-1}$  and  $C_{\text{d}} = 252 \mu\text{F cm}^{-2}$ ) was far smaller than that from  $\text{CO}_2$  adsorption ( $A_{\text{sp}} = 587 \text{ m}^2 \text{ g}^{-1}$  and  $C_{\text{d}} = 26 \mu\text{F cm}^{-2}$ ). This finding challenges the widely perceived pseudocapacitance resulting from the redox chemistry of the doping atoms [62]. In another recent study of a commercial activated carbon, argon was used as the adsorption gas, revealing an average pore size of  $0.9 \text{ nm}$  with  $92\%$  of the pores being  $<2 \text{ nm}$ . *In situ* NMR and electrochemical quartz microbalance (EQCM) were applied to study the relatively larger ions, i.e. the tetraethylammonium cation ( $\text{NEt}_4^+$ ) and tetrafluoroborate anion ( $\text{BF}_4^-$ ), in organic electrolytes. The findings correlate the applied electronic charge on the electrode very well with the responsive ionic charge in the pores, and confirm the charge storage mechanism to be the EDL capacitance [63].

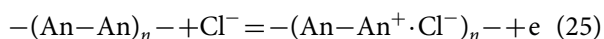
Although pseudocapacitance studies in modified or doped carbon materials are inconsistent as discussed above, it is clearer for some TMOs and ECPs. Electrochemical properties, particularly redox chemistry, of these materials were studied long before their use in supercapacitors. Such knowledge has been used in predicting the theoretical specific capacitance of these materials by the ratio of specific charge,  $Q_{\text{sp}}$ , and the potential window,  $\Delta E$ , of the material calculated according to equation (24).

$$C_{\text{sp}} = \frac{Q_{\text{sp}}}{\Delta E} + C_{\text{d}}A_{\text{sp}} = \frac{nF}{M\Delta E} + C_{\text{d}}A_{\text{sp}} \quad (24)$$

In this equation, the first term is the pseudocapacitance (cf. equation (21)) and the second term is the EDL capacitance (cf. equation (23)). Also, these two capacitive elements are assumed to be connected in parallel [39]. Obviously, the EDL term would only be significant for high  $A_{sp}$  materials, such as nanomaterials and highly porous carbons, but it is negligible in most other cases.

For  $MnO_2$ , the formula mass  $M = 86.937$  and  $n = 1$  for reaction (11) with  $x = 1$  and  $y = 0$ .  $\Delta E$  is experimentally determined from CVs and it is 0.85 V in Figure 6 (b). Without consideration of the EDLC, the theoretical value of  $C_{sp}$  can then be calculated to be 1305.68 F/g with  $F = 96\,485\text{ C mol}^{-1}$ . Note that the result from equation (24) depends on  $\Delta E$  which can vary between 0.8 and 1.0 V depending on materials and measurement conditions, which is possibly why different theoretical values of  $C_{sp}$  for  $MnO_2$ , such as 1100 and 1370 F/g, have been reported [64,65].

Similarly, the theoretical  $C_{sp}$  value can be calculated for ECPs, as explained by the following electron transfer reaction for polyaniline [39,66]



where An represents an aniline monomer unit in the polymer chain. When applying equation (24) to reaction (25), either  $M$  or  $n$  needs to be determined. This is because unlike a TMO, e.g.  $MnO_2$ , which can be well represented by a formula mass that can be associated with each electron transfer, ECPs are polymers and do not have a clear definition of formula mass. In reaction (25), two aniline monomer units are involved in each electron transfer, which is well known [39,66]. Considering that in a polymer chain, each aniline monomer has lost two protons,  $M = 2 \times (M_{\text{aniline}} - 2) = 182$ , where  $M_{\text{aniline}}$  is the formula mass of a free aniline molecule. The potential window for polyaniline to exhibit a rectangular CV is about 0.7 V which means  $C_{sp} = 757.34\text{ F/g}$  according to equation (24) without considering the EDL. In recent years, polyaniline has been prepared in various nanostructures, which means the contribution of EDL should be considered and the actually measured  $C_{sp}$  of nanostructured polyaniline may be higher than the theoretical value derived here for Faradaic process only.

Although equation (24) links the specific capacitance with the formula mass, the number of electrons in the Faradaic reaction, and the potential window, determination of these parameters is not always straightforward as exemplified by the polyaniline example. For example, if one compares the CVs of the  $MnO_2$ -CNT composite in Figure 6, it is clear that the charge transferred for either oxidation or reduction in the narrow potential range is about a half of that in the wide potential range. Thus, if the CVs in the wide potential range (which is 1.65 V in Figure 6(a))

corresponded to a one electron transfer reaction, it must have been a fractional number of electrons involved in the Faradaic reaction in the narrow potential range (0.85 V in Figure 6(b)). However, in the wide potential range, the CVs are peak-shaped and show poor reversibility and hence should not be used for capacitance analysis. More importantly, as discussed before, the peaked shaped CV is due to the change of Mn(III) to Mn(II), which means  $n = 2$  in the wider potential range.

It is acknowledged that several publications have claimed specific capacitance well over 1300 F/g in potential ranges narrower than 1.0 V for variously prepared  $MnO_2$  samples [67–69]. However, it is also noticed that these claims were made against measurements of extremely low loading of the  $MnO_2$  sample ( $<10\text{ }\mu\text{g cm}^{-2}$ ) on a flat electrode substrate, or loading the  $MnO_2$  sample on highly porous electrode substrate (e.g. the nickel foam). Consequently, these measurements would have inevitably included the EDL contribution from the electrode substrate.

Supercapacitors, either the EDLC or pseudocapacitor, are widely perceived to have high power capability, but low energy capacity in comparison with rechargeable batteries. However, if one considers equation (7) with a specific capacitance,  $C_{sp}$ , of 800 F/g, and a maximum voltage of 3.0 V for a symmetrical cell, the specific energy,  $W_{sp}$ , would be  $250\text{ Wh kg}^{-1}$ . This calculation obviously includes assumptions that are individually correct, but may not be realistic when they are considered in one device based on current literature. Specific capacitance higher than 800 F/g has been often reported for nanostructured pseudocapacitive materials, but the potential windows are rarely wider than 1.0 V, disregarding the electrolyte used. Thus, the asymmetrical design is a necessity to achieve higher voltages.

There are two main designs of asymmetrical devices. The first design is the so called asymmetrical supercapacitors in which both the positrode and negatrode are still capable of capacitive charge storage, but the combination can be (1) an EDLC electrode and a pseudocapacitance electrode (E||P), (2) two different EDLC electrodes (E1||E2), or (3) two different pseudocapacitance electrodes (P1||P2). The E1||E2 combination, such as ‘activated carbon (–) || graphite (+)’, is rarely reported in the literature [70] while the E||P and P1||P2 combinations are more popular, including ‘activated carbon (–) || polypyrrole-CNT (+)’ and ‘ $\text{SnO}_2$ -CNT (–) ||  $\text{MnO}_2$ -CNT (+)’ [11,54,71,72]. In most reported cases, increased charge capacity or cell voltage or both were achieved, leading to increased energy capacity. The use of composites of CNTs individually coated with either an ECP or TMO in supercapacitors is worth highlighting.

The achievements in production of various nanostructured materials are one of the important factors

contributing to the fast expansion of supercapacitor research in recent years. Among all nanomaterials used for making electrodes in supercapacitors, CNTs are unique and non-replaceable for their great structural, mechanical, electrical and chemical properties. CNTs are ideal for construction of porous structures with both micro- and nanometre sized and interconnected pores that are needed for passage of charge balancing ions. The high electrical conductivity of CNTs is also beneficial to fast movement of electrons within the electrode. Both the improved ionic and electronic conductivities are crucial for more complete utilisation of the active materials on the electrode in high speed charging and discharging. CNTs are mechanically very strong, which helps the redox active material coated on individual CNTs to withstand stress and fatigue caused by repeated intercalation and depletion of ions. This in turn prolongs the cycle life of the electrode materials. In terms of chemical properties, CNTs offer high stability towards various chemical and electrochemical attacks. However, they can undergo controllable partial chemical oxidation under acidic conditions. Such acid treated CNTs possess various surface oxygen containing functional groups that can help uniform dispersion of CNTs in an appropriate aqueous or organoaqueous solution up to or over 1 wt-% in concentration. The CNT suspension can then be introduced in various reaction media for coating with the desirable redox active materials.

Figure 9 presents electron microscopic images of as received CNTs and their composites with different redox active materials prepared by electrochemical co-deposition [47,73] redox deposition [44,74] and chemical precipitation [72]. Specifically, the progression of redox deposition of  $\text{MnO}_2$  on the CNT is illustrated in Figure 10. This chemical method has received particular attention recently because of the fast growing interest in preparation and application of composites of various metal oxides and carbon-based nanomaterials, e.g. CNTs, graphenes and silicon carbide [74–77].

The second design of asymmetrical devices is more dramatic by combining a supercapacitor electrode and a battery electrode into one device, although such devices have been reported under different names, mainly reflecting the different electrode materials used [9–14]. Clearly, using a unified approach, such as supercapattery (or superbattery) is desirable for development in research and commercial applications. The principle of supercapattery is schematically illustrated in Figure 2(d), but the advantage can be quantified further. As discussed above, it may be feasible to obtain a pseudocapacitive material with a specific capacitance value of 800 F/g, but it would be difficult to make a symmetrical supercapacitor from such a material to reach a cell voltage of 3.0 V or higher.

Now, consider a supercapattery with a lithium (Li) metal negatode and an activated carbon positrode. It is possible to predict the behaviour of the electrodes and the cell as shown by the GCDs in Figure 11(a). Obviously the cell behaviour is highly capacitive, and can therefore be dealt with using the capacitor equations, such as equation (5). It can be seen in Figure 11(a) that the minimum potential of the carbon electrode is 0.5 V vs.  $\text{Li}/\text{Li}^+$ , instead of zero. This is to prevent the carbon electrode from undergoing any lithiation during discharging.

To achieve the capacitive performance shown in Figure 11(a), the balance of the masses and hence charges of the positrode and negatode is important. In a supercapattery cell with a battery negatode and capacitor positrode, the charge passed through both electrodes must be the same, which in turn fixes the positrode to negatode mass ratio.

$$Q_- = m_- Q_{\text{sp}-} = m_+ C_{\text{sp}+} \Delta E_+ = Q_+ \quad (26)$$

$$\frac{m_+}{m_-} = \frac{Q_{\text{sp}-}}{C_{\text{sp}+} \Delta E_+}$$

For a lithium negatode,  $Q_{\text{sp,Li}} = nF/M_{\text{Li}} = 13\,900 \text{ C/g} = 3861 \text{ mAh g}^{-1}$  ( $M_{\text{Li}} = 6.941$ ,  $n = 1$ ). For the activated carbon positrode with  $C_{\text{sp,C}} = 200 \text{ F/g}$  and  $\Delta E = 4.0 \text{ V}$ ,  $Q_{\text{sp,C}} = C_{\text{sp,C}} \Delta E$ . The positrode to negatode mass ratio is  $m_+/m_{\text{Li}} = Q_{\text{sp,Li}}/(C_{\text{sp,C}} \Delta E) = 13\,900/(200 \times 4.0) = 17.375$ . As a result, the total mass of lithium metal used to build the supercapattery is negligible compared to that of the activated carbon. The specific energy of such a lithium-carbon supercapattery can be calculated using equation (5) in which  $C_{\text{cell}} \approx m_+ C_{\text{sp,C}}$ . As mentioned above, to avoid lithiation of the carbon positrode, discharging the lithium-carbon supercapattery can only reach a minimum voltage,  $U_{\text{min}}$ , instead of zero. Thus, equation (5) needs to be modified to equation (27) below.

$$W_{\text{sp}} = \frac{C_{\text{sp,cell}}}{2} (U_{\text{max}}^2 - U_{\text{min}}^2) \quad (27)$$

With the mass of lithium ignored,  $C_{\text{sp,cell}} \approx C_{\text{sp,C}} = 200 \text{ F/g}$ ,  $U_{\text{max}} = 4.5 \text{ V}$  and  $U_{\text{min}} = 0.5 \text{ V}$ , it can be calculated that  $W_{\text{sp}} = 555.6 \text{ Wh kg}^{-1}$ .

For a  $\text{LiC}_6 - \text{C}$  supercapattery, i.e. replacing the Li metal negatode with a lithiated carbon ( $\text{LiC}_x$ ,  $x \geq 6$ ) negatode, the theoretical specific charge capacity of  $\text{LiC}_6$  is 1340 C/g. Thus, the positrode to negatode mass ratio is  $m_+/m_{\text{LiC}_6} = Q_{\text{sp,LiC}_6}/(C_{\text{sp,C}} \Delta E) = 1340/(200 \times 4.0) = 1.675$  which means that the mass of the  $\text{LiC}_6$  negatode is not negligible. Because the cell still behaves in the capacitive way as shown in Figure 11(a), it is practically appropriate to estimate an apparent specific capacitance of the  $\text{LiC}_6$  electrode. Since the potential change of the  $\text{LiC}_6$  electrode is smaller than 50 mV along the potential plateau, the apparent specific capacitance should be larger than

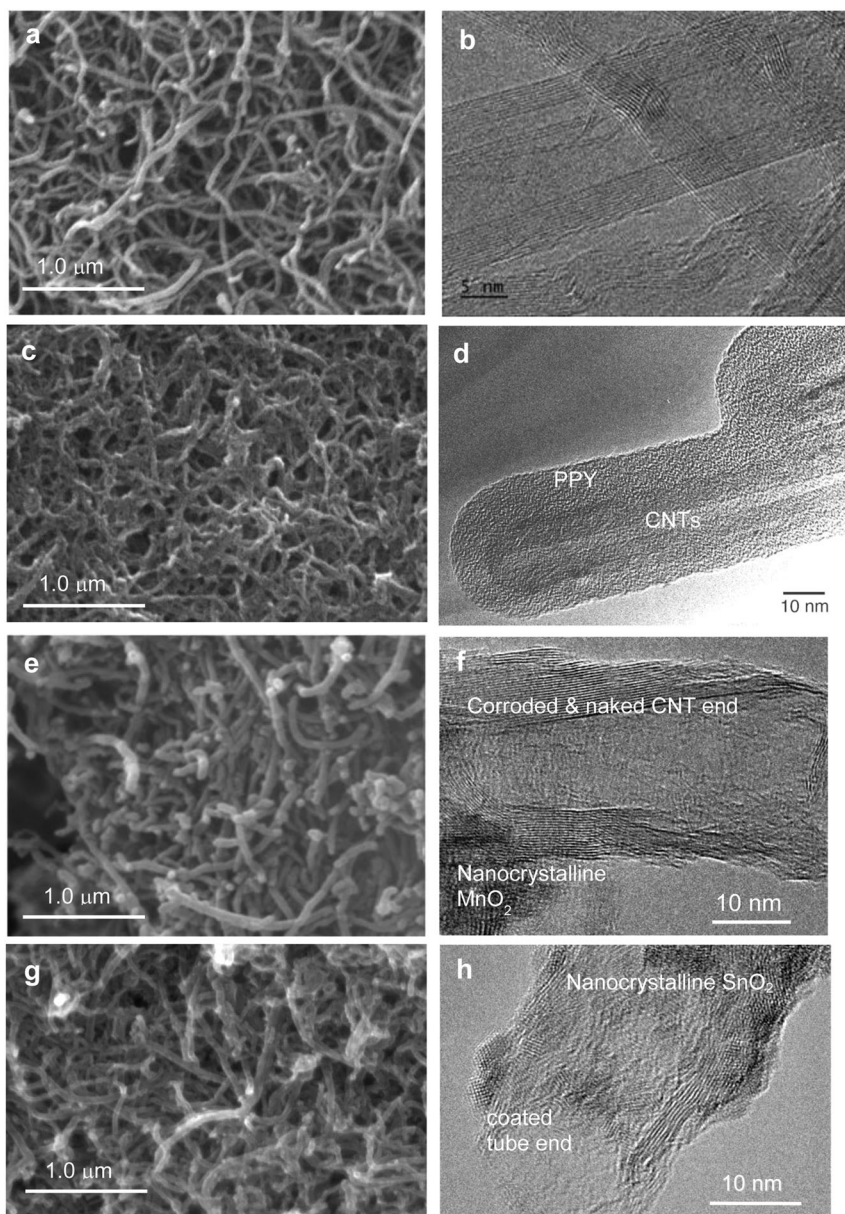


**Figure 9.** SEM (left) and HRTEM (right) images of CNTs before (a, b) and after coating with (c, d) polypyrrole by electrochemical co-deposition, (e, f) MnO<sub>2</sub> by redox deposition, and (g, h) SnO<sub>2</sub> by chemical precipitation [47,50,72–74].

1340/0.05 = 2680 F/g, which is over 16 times of that of the carbon positrode. Consequently, the cell capacitance is approximately the same as that of the carbon positrode. Assuming 1.00 g for the mass of the LiC<sub>6</sub> negatrode, the carbon positrode mass would be 1.675 g. It can then be derived that the specific cell capacitance is  $C_{sp,cell} = 1.675 \times 200 / (1.675 + 1.00) = 125.0$  F/g. Thus, for  $U_{max} = 4.5$  V and  $U_{min} = 0.5$  V, from equation (27), the specific energy of the LiC<sub>6</sub> – carbon supercapattery can be calculated to be  $W_{sp} = 347.2$  Wh kg<sup>-1</sup>.

In the two examples of supercapattery discussed above, the positrode is of the EDLC type with a relatively low specific capacitance but it has a wide potential range. If a positrode of the pseudocapacitive type is used with a higher specific capacitance (e.g.  $C_{sp+} = 500$  F/g), but a narrower potential range (3.5–4.5 V) as shown by the GCDs in Figure 11(b), the

positrode to negatrode mass ratio  $m_{pseudo}/m_{Li} = Q_{sp,Li} / (C_{sp,pseudo} \Delta E) = 13\,900 / (500 \times 1.0) = 27.8$  which is again large enough to neglect the lithium negatrode mass. Then, the specific energy can be calculated from equation (27) to be  $W_{sp} = 500 \times (4.5^2 - 3.5^2) / (2 \times 3.6) = 555.6$  Wh kg<sup>-1</sup>. Replacing Li metal by LiC<sub>6</sub> will lead to  $m_{pseudo}/m_{LiC6} = Q_{sp,LiC6} / (C_{sp,pseudo} \Delta E) = 1340 / (500 \times 1.0) = 2.68$ ,  $C_{sp,cell} = 2.68 \times 500 / (1 + 2.68) = 364.1$  F/g, and  $W_{sp} = 364.1 \times (4.5^2 - 3.5^2) / (2 \times 3.6) = 404.6$  Wh kg<sup>-1</sup>. These calculated results for cases as represented by Figure 11(b) compare very well with recent studies of the Li – MnO<sub>2</sub> cell as shown by the GCD in Figure 12(a), and also the Li-activated carbon and Li – RuO<sub>2</sub> cells with combined solid and aqueous electrolytes [7,8].

In reality, most battery electrodes work at potentials much more positive than those of the Li metal or LiC<sub>6</sub> compound negatrodes, and the respective CVs or GCD

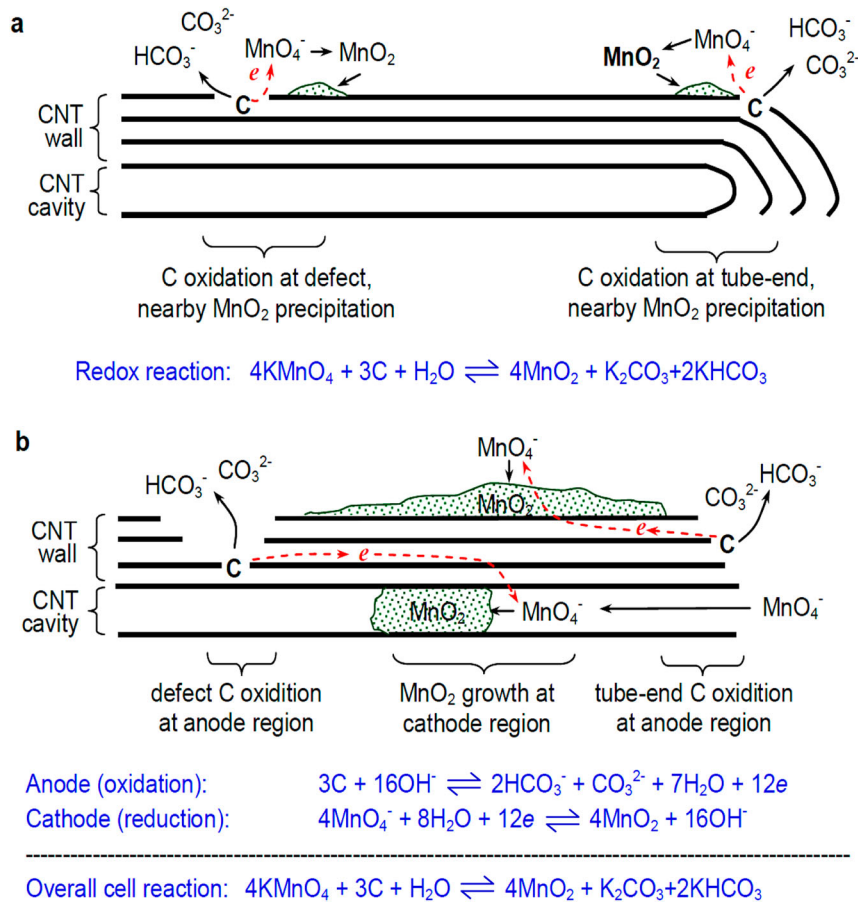


**Figure 10.** Illustration of redox deposition of  $\text{MnO}_2$  on CNT external and internal surfaces in two stages. (a) Stage 1: direct electron transfer reaction between  $\text{MnO}_4^-$  and nearby carbon at defect on CNT to deposit  $\text{MnO}_2$  near the defect. (b) Stage 2: formation of nanoscale micro-electrochemical-cell enables electron transfer from carbon at defect away from existing  $\text{MnO}_2$  coating (formed in Stage 1) via CNT wall to  $\text{MnO}_4^-$  to further grow the  $\text{MnO}_2$  coating and filling at external or internal surfaces of the CNT [44,74].

plots are often observed to be much more sluggish [6,36,80]. As a result, the capacitor concept and equations should not be applied. Figure 11(c) shows the calculated GCDs of the electrode potential and cell voltage against the charging and discharging times. In this case, because of the sluggish GCD of the battery negatrod, and also the pseudocapacitive electrode potential being not very much more positive than those of the negatrod, the GCD of the cell is non-linear. In such cases, the energy capacity of the cell should be obtained by integration of the GCD of the cell. Graphically, the energy capacity is proportional to the area under the discharging branch of the GCD. Obviously, the GCDs in Figure 11(c) are more similar to those of batteries than supercapacitors. Therefore, it may be worth calling these devices as supercattery to differentiate from supercapattery which behaves more like a supercapacitor.

In summary, the combination of battery and supercapacitor electrode materials into one EES devices can result in behaviour that can be either apparently the same as that of a capacitor showing the linear voltage variation with time as displayed in Figure 11(a and b), or very much comparable to that of a battery with the voltage-time relation being non-linear. In each of

these cases, the shaded area under the discharging branch of the GCD of the cell is proportional to the energy discharged. Equations (5) or (27) can be applied to the cases of linear GCDs, but not to the non-linear ones. Integration of the non-linear plot is the only way to obtain the energy value. Such hybrid devices are not the same as either the conventional supercapacitor or battery in terms of charge storage mechanisms but capable of improved technical performances. The number of such hybrid devices is growing exponentially and hence deserve new names in collection which is why supercattery and superbattery have been proposed.

### Materials for supercattery

The EES literature is largely filled with research findings from synthesis of new electrode materials and/or tests of these in a particular EES environment or directly in an EES device, while most recent efforts have been devoted to construction of various nanostructures [10,11,13,14,16,17,23–31,34–39,44–51,53–58,60–62,64–70,72–77,80]. These efforts have undoubtedly contributed to the progress in EES research and development, but it is still necessary to link material design, synthesis and selection with the

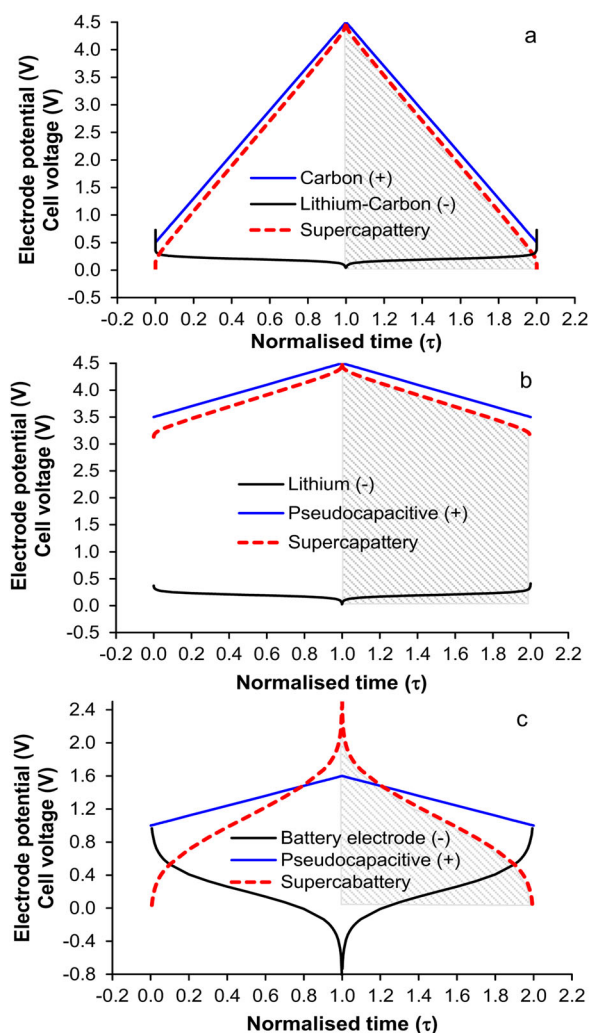


**Figure 11.** Calculated electrode potential (black and blue lines) and cell voltage (red dashed lines) as a function of normalised time for galvanostatic charging and discharging of three types of supercapattery with (a) a negatrod of lithium metal or lithiated carbon and a positive positrod of activated carbon, (b) a negatrod of lithium metal or lithiated carbon and a pseudocapacitive positrod, and (c) a negatrod of the typical battery type and a pseudocapacitive positrod [3,5,6,78].

needs to promote electrode processes and reactions for charge and energy storage.

Technically, all EES devices should consider three important factors, i.e. energy capacity, charging and discharging speed (or power capability) and cycle life. The above discussion has focused mainly on energy capacity, which is more intrinsically determined by the material properties that are closely related to thermodynamics, e.g. equations (19) and (22). In practice, the realisation of thermodynamic energy capacity, particularly in a repeated manner, is strongly dependent on the electrode kinetics of the charging and discharging processes or reactions.

Electrode kinetics studies firstly the *transfer* of charges (electrons and/or ions) at the boundary (interface or interline) between the electrode (electronic conductor) and one or more condensed phases (semiconductor and ionic conductor) connected to the

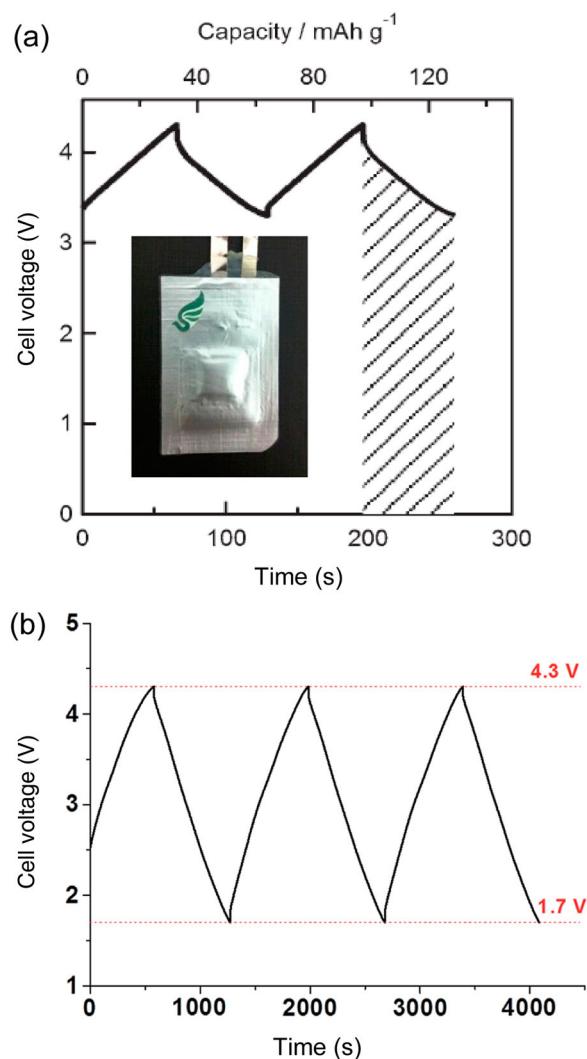


**Figure 12.** Experimental demonstration of supercapatteries with GCDs from (a) (–) Li | solid electrolyte | aqueous electrolyte | MnO<sub>2</sub> (+) (0.255 mA cm<sup>-2</sup>) [7] and (b) (–) Li | ionic liquid | activated carbon (+) (1 mA cm<sup>-2</sup>) [79]. Inset in (a) is a photograph of the fabricated pouch cell [8]. (Redrawn and reprinted with permission from the Royal Society of Chemistry and Elsevier).

electrode (e.g. the ‘metal (electrode) | electrolyte’ interface, or the ‘carbon | metal oxide | electrolyte’ interline), and secondly the *transport* of charges (and the associated masses) through one or more of the condensed phases (e.g. transport of anions in the aqueous electrolyte of a porous polypyrrole electrode). In practice, charge transfer and transport processes are always correlated (to satisfy the neutrality requirement) and often mutually influential. However, some variables (e.g. chemical nature of material and electrode potential) affect more on charge transfer, and the others (e.g. porous structure of material and temperature) exert more impact on charge transport.

Manipulation of charge transfer kinetics can be achieved by selection of the electrode active material. For example, direct use of Li metal as the negatrod is based on electron transfer between the Li metal and Li<sup>+</sup> in the electrolyte, accompanied by deposition and dissolution of the Li metal. The same occurs on

the lead (Pb) metal negatrod. In absence of deposition and dissolution, many TMOs and ECPs can enable electron transfer in capacitive and non-capacitive Faradaic charge storage, while carbons of different porous and nano structures affect mainly ion transfer in capacitive non-Faradaic charge storage. For TMOs, except for single or few atomic or molecular layers, electron transfer occurs at the 'current collector | TMO' interface and it is always accompanied by ion transfer at the 'TMO | electrolyte' interface to maintain the electrical neutrality inside the electrode active material. A similar picture can also be seen in cases of various ECPs. Obviously, between these two interfaces electron and ion can transport inside the active material to maintain electric neutrality.

In all EES devices, except for metal deposition and dissolution, and ultrathin layers (single and few atomic or molecular layers), charge transport kinetics is far more relevant to ion transport than to electron transport. The kinetics depends more strongly on ion movement inside the active material on the electrode than in the bulk electrolyte. Because ion movement in a solid phase is far slower than in a liquid electrolyte phase, porous and nanostructured materials are preferred so that the depth of ion transport inside the solid phase is minimised. It is worth mentioning that  $\text{RuO}_2$  is a rare example as a good conductor of both electrons and ions (protons), but this is not the case for most TMOs and ECPs. Thus, formation of a composite of the TMO or ECP with an electronically conducting support that can also help construction of a porous structure is an efficient approach. For such purposes, nanostructured carbon materials, such as CNTs and graphenes, are the popular support materials, as exemplified in Figure 9 for composites of CNTs and TMOs or ECPs. Synthesis of these composite materials is also relatively simple. A good example is redox deposition for preparation of composites of CNTs and  $\text{MnO}_2$  as illustrated in Figure 10.

It should be emphasised that although porous nanostructures facilitate significantly ion transport kinetics, they may not necessarily help improve the material stability for repeated charging and discharging cycles. Theoretically, all electrode active materials for Faradaic charge storage will suffer from fatigue damages due to repeated ingress and egress of ions. The effective way to mitigate this intrinsic problem is to support the active material as a thin coating on electrochemically inert nanoparticulates. Again, CNTs and graphenes are ideal candidates for loading both TMOs and ECPs [64–66,72–77]. There are also attempts to support the active materials on other inorganic nanomaterials to help not only ion transport kinetics and material stability, but also to exert desired chemical interactions with the active material [81,82]. A fairly successful example was recently reported for coating  $\text{MnO}_2$  on nanowires of  $\text{CeO}_2$  and the test of

the  $\text{MnO}_2$ - $\text{CeO}_2$  composite positrod in an asymmetrical supercapacitor with an oxidised graphene negatrod in an aqueous electrolyte of  $1.0 \text{ mol L}^{-1} \text{ Na}_2\text{SO}_4$  [81]. However, such approaches often suffer from the poor electronic conductivity of these inorganic nanomaterials.

In EES technologies, not only the solid electrode materials are important, but also the liquid electrolytes which are mainly aqueous, organic and IL electrolytes. Aqueous electrolytes are advantageous in their high conductivity and heat capacity, and low cost and environmental impact. The low decomposition voltage of water (*ca.* 1.2 V) is often quoted to discourage application of aqueous electrolytes. This perception is unfortunate because it is actually possible to extend the cell voltage of aqueous supercapacitors by employing electrode materials with high overpotentials for evolution of either or both hydrogen and oxygen gases. The classic lead-acid battery contains an aqueous electrolyte (concentrated  $\text{H}_2\text{SO}_4$ ) but works at a voltage of *ca.* 2.2 V, while recent reports also show cell voltages around 2.0 V for supercapacitors with carbon-based negatrod and  $\text{MnO}_2$  based positrodes in neutral aqueous electrolytes, such as  $\text{Na}_2\text{SO}_4$  [38,81,83,84]. It should be pointed out that using electrode materials with high oxygen and hydrogen overpotentials does not necessarily mean a high supercapacitor voltage would definitely be achieved. The capacitance ratio or mass ratio of the positrod to negatrod of the supercapacitor must also be adjusted properly so that the potential ranges of the negatrod and positrodes can be fully utilised [38,83–86]. Another perception is that water freezes at  $0^\circ\text{C}$ , and hence aqueous electrolytes could not be used at low temperatures. In fact, many inorganic salts can help decrease the freezing temperature of water significantly, as shown in Figure 13(a) [87]. The CVs in Figure 13(b and c) demonstrate a CNT electrode retaining its capacitive charge storage ability at temperatures below  $-60^\circ\text{C}$  in an organoaqueous electrolyte of  $\text{CaCl}_2$  [88].

Organic electrolytes, such as tetraethylammonium tetrafluoroborate dissolved in acetonitrile or propylene carbonate, are currently used in commercial supercapacitors with activated carbon electrodes [89–91]. They offer wide potential and temperature windows (up to 3.5 V, from  $-50$  to  $70^\circ\text{C}$ ). Cost of organic electrolytes is not low but affordable for commercial purposes. Nonetheless, organic solvent based electrolytes are usually highly flammable, which causes safety concerns, particularly when the EES device is to work at high charging currents and high cell voltages. Problems with organic electrolyte based Li-ion batteries are often reported [92,93], and the same or similar situations are expected for supercapacitors with organic electrolytes.

To enable safe operation at cell voltages higher than 4.0 V, the use of solid ion conducting membranes

together with aqueous electrolytes has been demonstrated [7,8]. This approach will progress further if the ionic conductivity, mechanical stability, and manufacturing flexibility and cost of the solid ion conducting membrane can be significantly improved. In fact, the technically more desirable choices to achieve high cell voltages are perhaps ionic liquids (ILs) which have promised potential windows of 4–6 V and also low evaporability and flammability [94–99]. ILs have long been investigated for electrochemical applications for both materials and energy purposes. Tests of ILs in lithium ion batteries have revealed promising results [99] but ILs are in fact and incidentally better for supercapacitors and supercapatteries. This is because, in principle, the cell voltage of a rechargeable battery

is fixed by the potential difference between the two electrode reactions, but it is by the decomposition voltage of the electrolyte in a supercapacitor or supercapattery. In line with this understanding, a symmetrical supercapacitor with electrodes of curved graphene sheets and an IL electrolyte of 1-ethyl-3-methylimidazolium tetrafluoroborate was tested to a cell voltage of 4.5 V. The specific energy was reported to be  $90 \text{ Wh kg}^{-1}$  at room temperature but increase to  $136 \text{ Wh kg}^{-1}$  at  $80^\circ\text{C}$  [100]. Note that this temperature assisted increase in specific energy is a reflection of the drawback of ILs: they are often highly viscous at room temperature and their component ions are slow moving and unable to access all the internal surfaces of the graphene electrode.

Application of ILs in supercapattery is still rare in the literature, but it can be expected to benefit from the accumulated knowledge of lithium ion battery research. In the author's laboratory, preliminary tests of a supercapattery with a lithium negatrod, an activated carbon positrod (110 F/g) and an IL electrolyte of  $\text{LiClO}_4$  revealed a maximum cell voltage of 4.2 V with the minimum discharging voltage being 1.7 V. The GCD of this IL supercapattery is shown in Figure 12(b) from which it was derived that the specific energy reached beyond  $230 \text{ Wh kg}^{-1}$  [79]. It can be anticipated that if the specific capacitance of the positrod may be increased to over 400 F/g by using a pseudocapacitive material, the specific energy of the IL based supercapattery can be even higher as already discussed above in relation with Figure 11(b).

Apart from the above discussed electrode materials and electrolytes which play active roles in EES devices, there are other materials as illustrated in Figure 2, including the separator, current collector and packaging materials [37]. These materials do not in principle participate in the charging and discharging processes, but their presence in the EES devices enable and even can in some cases enhance the performance of the active materials. Nevertheless, because of their relatively inert nature, enabling materials are selected more because of their commercial availability and costs, and hence have attracted little research attention. Fortunately, these enabling materials perform similarly in, and can be shared between different types of EES devices. For example, in the author's laboratory, it was found that supercapattery could use the same porous polymeric separators (membranes) for supercapacitor with either an aqueous or organic electrolyte. These separators include common laboratory filter papers [71] and commercial membranes such as the Celgard products [50] which are originally produced for use in Li-ion batteries. Ion selective membranes are rarely used in supercapacitor or supercapattery because they are far more resistive than the conventional porous polymer membranes. However, to enable the use of Li metal as the negatrod in aqueous EES

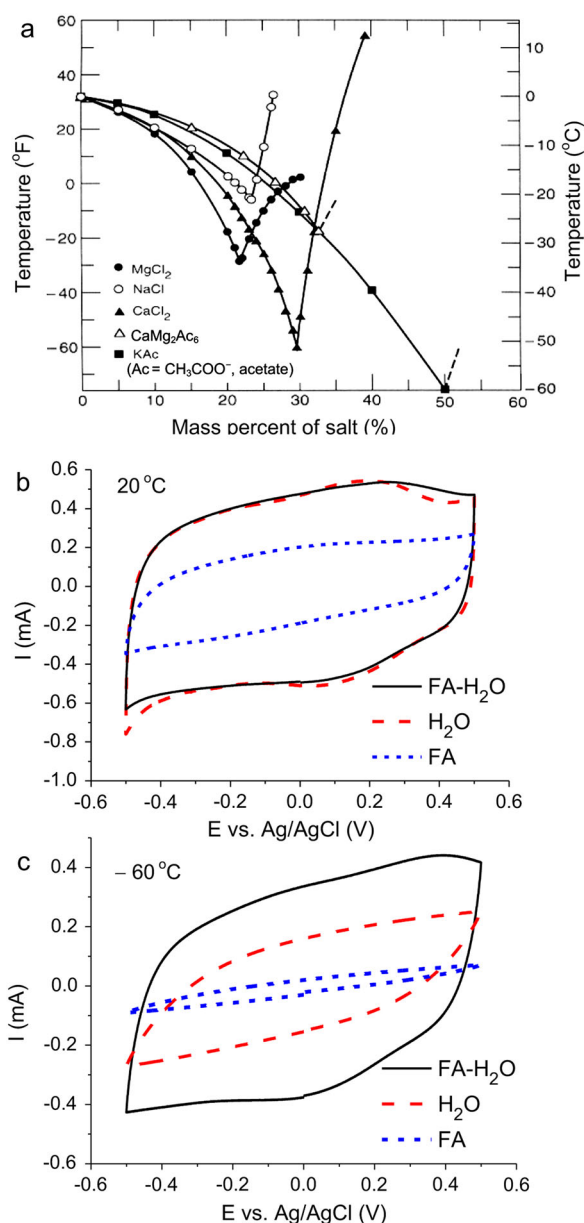


**Figure 13.** (a) Phase diagrams of  $\text{H}_2\text{O}$  and  $\text{CaCl}_2$ ,  $\text{MgCl}_2$ ,  $\text{NaCl}$ ,  $\text{CaMg}_2\text{Ac}_6$ , or  $\text{KAc}$  [87]. (b, c) CVs of a CNT electrode at (b)  $20^\circ\text{C}$  and (c)  $-60^\circ\text{C}$  in the  $\text{CaCl}_2$  solution of FA ( $1.0 \text{ mol L}^{-1}$ ),  $\text{H}_2\text{O}$  ( $2.0 \text{ mol L}^{-1}$ ) and mixed FA- $\text{H}_2\text{O}$  (1:1, v:v,  $2.0 \text{ mol L}^{-1}$ ). Potential scan rate:  $100 \text{ mV s}^{-1}$  [88]. (FA: formamide).

devices, solid  $\text{Li}^+$  ion conductor remains the preferred choice [7,8]. The current collector materials used in rechargeable batteries, e.g. carbon plate, aluminium foil and nickel foam, find good applications in supercapacitors and supercapatteries. The author and co-workers found that titanium foils performed very well in chloride based aqueous electrolytes [50,71] but could suffer from passivation in sulphate containing electrolytes. Last but not the least, packaging materials not only support the structure of EES devices, but also isolate the EES device from its environment to avoid solvent evaporation and prevent moisture from entering the cell. Thermal lamination with thermoplastic films is an effective way to seal off relatively small EES devices. However, for large devices, particularly those stacks of multiple cells, more sophisticated designs and constructions are necessary. An attempt made in the author's laboratory is discussed in detail in the next section.

### Prospects and challenges

Investigation and application of EES devices are experiencing unprecedented innovation and development opportunities, thanks to the urgent need to mitigate the detrimental impact of anthropogenic  $\text{CO}_2$  emission, and to utilise renewable sources in places of the fossil resources. In this line, because electricity is not a naturally available form of energy, EES development needs to suit both traditional and new electricity generation and transfer technologies, such as coal fired and nuclear power plants, and photovoltaic and wind farms. Even for storage, EES can be competitive with, but more often complementary to mechanical (pumped hydro, compressed air) and thermal (phase change materials, molten salts) energy storage. In comparison with other storage methods, EES devices are

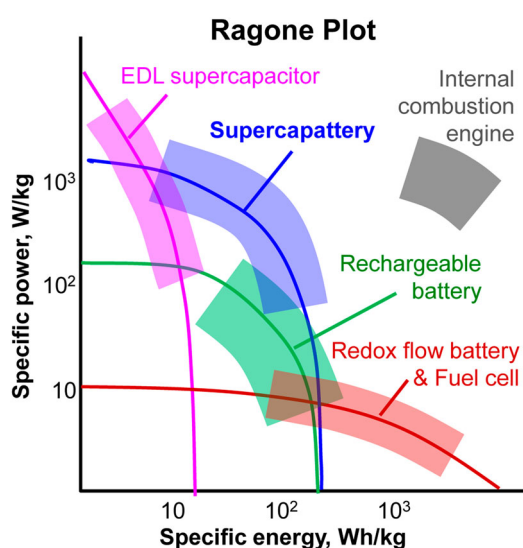
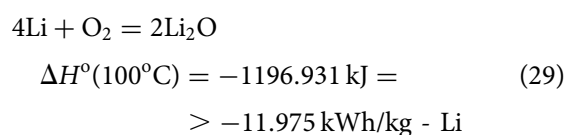
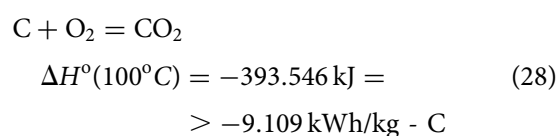


**Figure 14.** A schematic Ragone plot showing the position of supercapattery relative to other energy technologies [46].

unique for their modular nature and hence applicable at both small and large scales and for both stationary and mobile purposes.

As discussed in previous sections, a great many past efforts have focused on increasing the energy and power densities of individual EES cells, which is mostly driven by the need for mobile or transport applications. In this line, supercapattery offers great promises by combining the merits of supercapacitor and rechargeable battery. Based on the current literature and the research progressing in the author's laboratory, schematic Ragone plots are drawn in Figure 14, showing the relative position of supercapattery in relevance to several EES devices and internal combustion engine. Note that Figure 14 reflects practically achieved energy and power correlations, at least in laboratory. This is well reflected by the position of internal combustion engine being far away from those of the EES devices presented. In principle, the specific energy of battery can reach that of internal combustion engine. This can be shown straightaway by the following two reactions and the related specific enthalpy changes.



Reaction (28) occurs in the coal fired power plant, while reaction (29) in the lithium metal – air battery. (Reactions (28) and (29) are the same as reactions (12) and (18), but are shown here for discussion convenience at a different temperature.)

In reality, the energy released from both reactions cannot be fully utilised to do work because of the Carnot cycle restriction for reaction (28), and various polarisation losses for reaction (29). Note that reaction (28) can be utilised to build a carbon-air battery which is the same as the so called direct carbon fuel cell [101]. Therefore, one may electrochemically reverse both reactions (28) and (29), which is equivalent to charging the respective battery. In such a charging process, further energy losses are inevitable due to various polarisations. As a result, the specific energy of a rechargeable battery is lower than that of the primary battery, and much lower than the thermodynamic prediction.

However, the above analysis does not mean that current EES technologies have no room for improvement. This is typically demonstrated in the significantly improved lithium metal – air battery that used a graphene oxide electrode,  $\text{LiI}$  as the redox mediator to

prevent over charging, and the solvent dimethoxyethane to help reversible formation and removal of crystalline LiOH during charge and discharge [102]. An energy efficiency of over 93% was claimed together with an energy capacity of  $5760 \text{ Wh kg}^{-1}$  (cf. discussion relevant to reaction (18) and equation (19)), while the number of charge–discharge cycles reached over 2000 at the rate of 1 A/g-carbon. On contrary to previous efforts that emphasise avoidance of moisture in experiments involving lithium metal, the formation and removal of LiOH was assisted by presence of moisture in the solvent.

Continuous innovation in electrolyte, such as solid lithium (or sodium) ion conducting membranes, task-specific ILs and organoaqueous solutions of low freezing temperatures, promises new EES devices and improved performances, as discussed above. In these cases, the challenges remain to increase the ion conductivity of the solid ion conducting membrane and ILs, and to increase the potential window of the organoaqueous solutions.

Undoubtedly, the use of nanostructured materials in EES devices has helped significant progresses in terms of storage capacity, power capability and cycling stability. A special credit goes to CNTs and graphenes which are perhaps the most studied nanomaterials for EES, either used alone or, more often, formed composites with redox active materials, such as ECPs and TMOs. In these composites, CNTs and graphenes play very similar electrical, chemical and mechanical roles, but they may differ significantly in terms of structural effects. When CNTs and their composites are made into an electrode, it is impossible to compact very much these nanofibrils, which is beneficial to formation of a porous electrode. This is clearly shown in Figure 9. In fact, in the author's laboratory, CNT-PPy discs of a few millimetres in thickness have been successfully tested for capacitive charge storage.[103] For graphenes, these two dimensional nanosheets can pack into a dense structure via face-to-face stacking, which would not be helpful to ion conduction. This prediction has found evidence as shown in Figure 15 which is discussed in more detail below.

In response to the concern on the stacking of graphene sheets, an elegant design and successful experimental tests were reported recently in which films with graphene oxide sheets packed densely in parallel were obtained from drying concentrated suspensions [104]. Such obtained films were then rolled into cylinders as shown in Figure 15(a). The cylinder was then cut into thin discs at  $-40^\circ\text{C}$  with a rotary cryomicrotome to avoid damage to the cross-section during cutting. The graphene oxide discs were then reduced at elevated temperatures up to  $1000^\circ\text{C}$ , which removed the oxygen atoms and left sufficient gaps between the parallel graphene sheets. After reduction, the graphene disc was attached to the surface of the electrode (current collector), creating vertically aligned graphenes

on the electrode surface. Such an electrode structure is desirable for both electron and ion conduction. Consequently, rectangular CVs were recorded at high potential scan rates, up to  $20 \text{ V s}^{-1}$ . In comparison, horizontally stacked graphene sheets suffered from much inferior electrochemical performances as shown in Figure 15(b). Such a huge difference can be attributed to, as predicted above, the vertically aligned graphenes being friendly to ion transport, in contrast to the horizontally stacked graphenes making it difficult for ion ingress. Figure 15(c) offers schematic illustration of this understanding which is further confirmed by the SEM images of the two electrodes with differently oriented graphene layers. It should be mentioned that in this work, 5% single walled CNTs were mixed with the graphene oxide to prevent unwanted close stacking between graphene sheets and also to help improve conductivity. There are nonetheless technical questions, such as how practical this rolling and cutting method can be for commercial application.

Further, innovation in device design and engineering is another area for technology growth. It is in this line that supercapattery (or in other names) has been proposed and demonstrated in the past decade or so. The two examples mentioned above in combining the Li metal negatode and a capacitor positrode into a supercapattery is promising in technical terms, but resources for Li are restricted. Alternatively, many nanostructured materials, such as the  $\text{Ni}(\text{OH})_2$ -graphene composite mentioned above, were incorrectly claimed to possess high specific capacitance. However, these new battery electrode materials indeed presented much improved charge transfer and transport kinetics and also cycling durability and stability. Combination of such a nanostructured battery type electrode with a capacitor electrode is another approach for supercapattery design, and the current literature offers many choices. For example, the design of a new supercapattery can be based on Figure 16(a) which shows the CV of a negatode of chitosan derived nitrogen doped activated carbon (N-AC) [105] together with that of the  $\text{Ni}(\text{OH})_2$ -graphene positrode [42] in concentrated KOH electrolytes. The specific capacitance of N-AC was reported to be as high as  $252 \text{ F/g}$  in a potential range of 0 to  $-1.0 \text{ V}$ , and the specific charge capacity of  $\text{Ni}(\text{OH})_2$ -graphene could be derived to be about  $730 \text{ C/g}$ . According to the same principle of equation (26), it can be derived that the positrode to negatode mass ratio of the new supercapattery should be  $m_+/m_- = C_{\text{sp-}} \cdot \Delta E_- / Q_{\text{sp+}} = 252 \cdot 1.0 / 730 = 0.35$ . This mass ratio would enable the cell voltage to reach the sum ( $1.55 \text{ V}$ ) of the potential ranges of the two electrodes as shown in Figure 16(a). It has been discussed above that the strategy of unequalisation of electrode capacitances can significantly increase cell voltage and hence the energy capacity of supercapacitor and also supercapattery [38,85,86]. In Figure 16(a), the

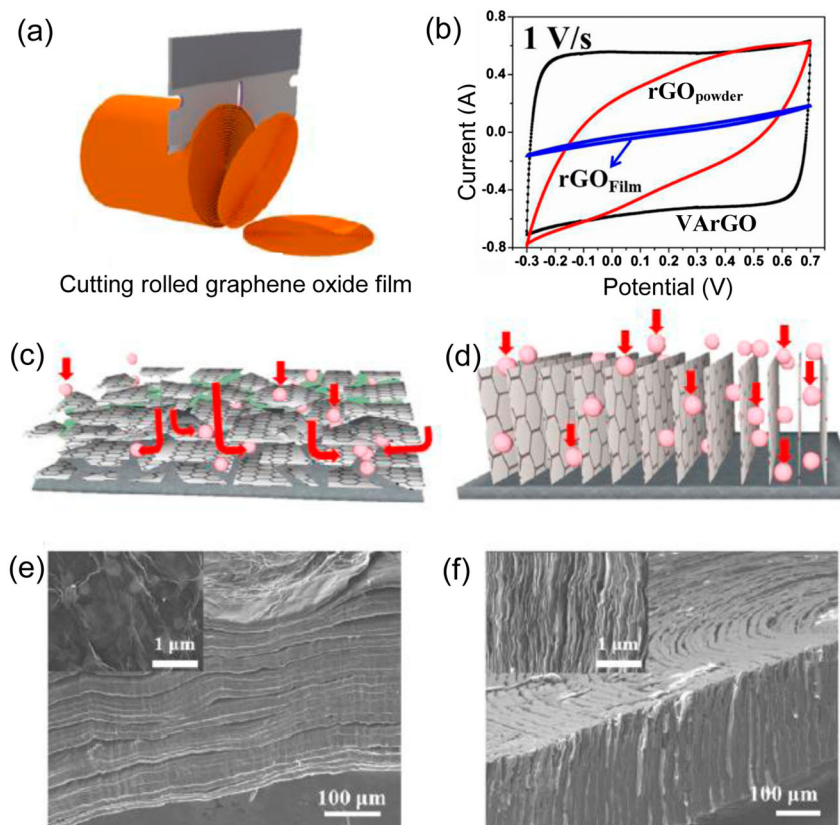


**Figure 15.** (a) Schematic illustration of cutting rolled film of graphene oxide with 5 wt-% SWNTs as spacer into thin discs that can be thermally reduced and made into electrodes with vertically aligned reduced graphene oxide (VArGO). (b) CVs of VArGO (black line), rGO<sub>powder</sub> (red line) and rGO<sub>film</sub> (reduced graphene oxide powder and film) in the 6 mol L<sup>-1</sup> KOH solution. (c, d) Cartoons of interactions of ions with (c) horizontally stacked (rGO<sub>film</sub>) or (d) vertically aligned VArGO graphene layers on electrode. (e, f) SEM images of (e) rGO<sub>film</sub> and VArGO [104]. (Redrawn and reprinted with permission from American Chemical Society).

potential range of N-AC may still be extended negatively. If so, it is possible to reduce the mass loading of N-AC on the negatrod to increase the supercapattery voltage beyond 1.55 V.

Obviously, there are many other choices from the current literature for selection of materials, pairing of electrodes and design of supercapattery, and the general strategy is summarised in Figure 16(b). In comparison with Figure 2(d), more options for construction of supercapattery are presented in Figure 16(b), including both asymmetrical and symmetrical designs. Of these, an interesting and rarely studied design is the symmetrical device with materials capable of non-capacitive Faradaic charge storage or simply Nernstian storage. Such a symmetrical device can be achievable and working if the electrode reaction is sufficiently reversible, unlike the example given in Figure 8. Because Nernstian storage occurs in a relatively narrow potential window, the symmetrical device with a Nernstian electrode material would also have a relatively small cell voltage. Alternatively, the symmetrical device may be built with a material capable of oxidative and reductive charge storage, respectively, at well separated positive and negative potentials. In this line, a recent study of the hierarchically nanostructured composite of NiO (micro-flower) and In<sub>2</sub>O<sub>3</sub>

(nano-rod) in the aqueous electrolyte of 3 mol L<sup>-1</sup> KOH revealed very satisfactory charge storage capacity (213 mAh g<sup>-1</sup> at 5 A/g), good rate capability (79 mAh g<sup>-1</sup> at 30 A/g), and desirable cycle stability (21% capacity loss after 50 000 cycles at 10 A/g) [106].

An interesting result from this study is the construction of a symmetrical supercapattery using the NiO–In<sub>2</sub>O<sub>3</sub> composite [106]. In a potential window of –0.2 to 0.6 V, the composite exhibited CVs, as shown in Figure 17(a) which was recorded in a three electrode cell, that are fairly comparable to that in Figure 8(a). It can be seen that the oxidation and reduction peaks are well separated, which is indicative of low reversibility and implies that the composite would not be suitable for construction of a symmetrical device. However, when assembled into a two electrode symmetrical cell, the cell voltage could be surprisingly scanned between 0 and 1.5 V and the CVs were of a very different shape as shown in Figure 17(b). The GCDs in the same voltage range in Figure 17(c) also suggest different electrode reactions from those shown in Figure 17(a). A further study of the NiO–In<sub>2</sub>O<sub>3</sub> composite revealed interesting charge storage reactions at both the positive (0–0.6 V) and negative (0 to –1.3 V) potentials, see Figure 17(d). While this finding explains the differences between the CVs in Figure 17(a and b), the NiO–In<sub>2</sub>O<sub>3</sub>

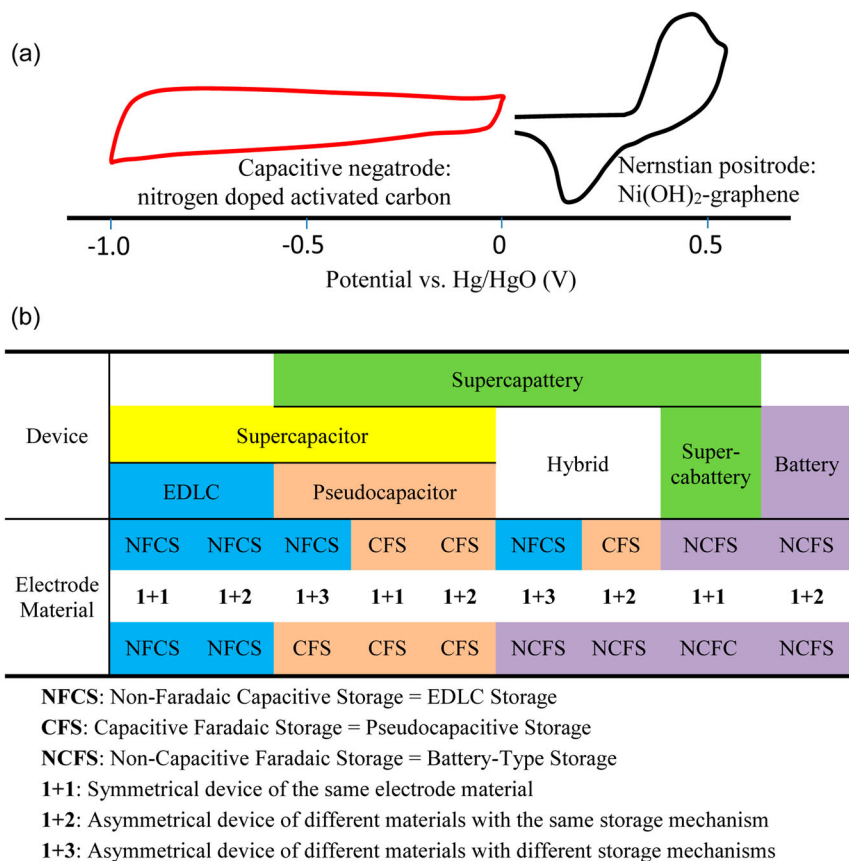


**Figure 16.** (a) CVs of the  $\text{Ni}(\text{OH})_2$ -graphene composite (black line) [34] and the chitosan derived nitrogen doped activated carbon [105] in concentrated aqueous KOH electrolyte (Redrawn from refs. 34 and 105). (b) Ways of pairing the same or different electrode materials into supercapacitor, battery, supercapattery or supercabattery [78].

composite represents a rare example of oxide based materials capable of charge storage at both and well separated positive and negative potentials. Similar properties have been long known for various polythiophenes which form symmetrical cells with the cell voltage exceeding 3 V in organic electrolytes. Unfortunately, these polymers alone are unstable in long term cycling [26]. Another point worth noting is that such symmetrical devices could be discharged to 0 V (cf. Figure 17(b and c)), which is a main feature of supercapacitor and supercapattery, but it is absent among conventional rechargeable batteries.

Another engineering approach is shown in Figure 18(a), illustrating the application of bipolar plates (current collectors) in assembly of two individual EES cells, particularly supercapacitors or supercapatteries, via internal serial connections [50,71]. An important component not shown in Figure 18(a) is the sealing ring between each pair of the bipolar current collector plates. In principle, multiple cells can also be serially stacked via the bipolar plates. While such a multiple cell stack is able to output a much higher voltage than a single cell, it is also a low cost way to increase the specific energy (or energy density) of the EES device. This can be explained as follow. To connect  $N$  cells in series, the number of current collectors is

$2 \times N$  for external connection, but it is  $N + 1$  if the cells are connected internally via bipolar plates. Obviously, when  $N$  is sufficiently large ( $\geq 10$ ), the weight of the  $N$  cells with bipolar connection will be significantly lower than that of externally connected  $N$  cells, leading to increased specific energy.

A concern on such a stack of multiple cells internally connected in series is that if one of the cells is malfunctioning, the whole stack may malfunction as well. This seems a valid concern, but it needs practical justification. On the contrary, in the author's laboratory, measurements of a stack of 19 supercapacitor cells with internal bipolar connections revealed ideal capacitive CVs and GCDs as shown in Figure 18(b and c). Further, although this 19 cell stack was manually fabricated, its equivalent series resistance (ESR) is as low as 0.3 ohm, as determined by electrochemical impedance spectroscopy, see Figure 18(d). This corresponds to a maximum power  $[=U^2/(4 \times \text{ESR})]$  of 333 W, or 24 kW kg<sup>-1</sup> against the total material mass on all electrodes. Obviously, these ideal capacitive performances manifest the absence of any malfunctioning cell in the stack. In commercial practice, because each component in the stack is simply planar in shape, as shown in Figure 18(a), good manufacturing reproducibility can be conveniently achieved in modern production lines.

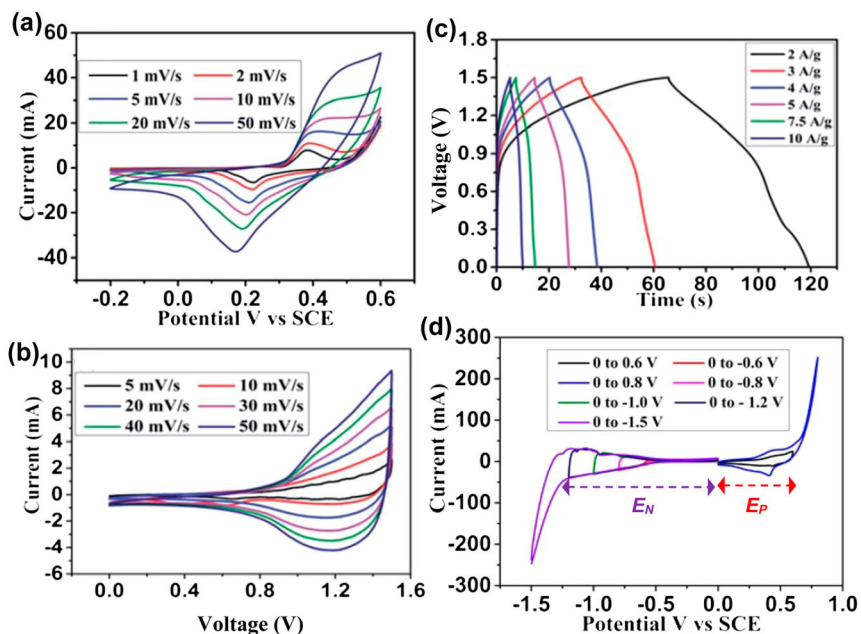


**Figure 17.** CVs of (a) a single electrode and (b) a symmetrical cell of the NiO-In<sub>2</sub>O<sub>3</sub> composite at the indicated scan rates. (c) GCDs of the symmetrical cell. (d) CVs of the negatrotde ( $E_N$ ) and positrotde ( $E_P$ ) in the symmetrical cell measured in different potential ranges with a reference electrode. Electrolyte: 3.0 mol L<sup>-1</sup> KOH [106]. (Redrawn and reprinted with permission from the Royal Society of Chemistry).

## Summary

This article has given a critical review of recent progresses in research and development of EES technologies, focusing on supercapacitor and supercapattery as a generic term for all designs combining the merits

of rechargeable battery and supercapacitor. In addition to a brief introduction of the electrochemical basics for EES, common terminologies used in EES literature are explained to help clarify some confusion in relation with the use of cathode and anode in places of positive

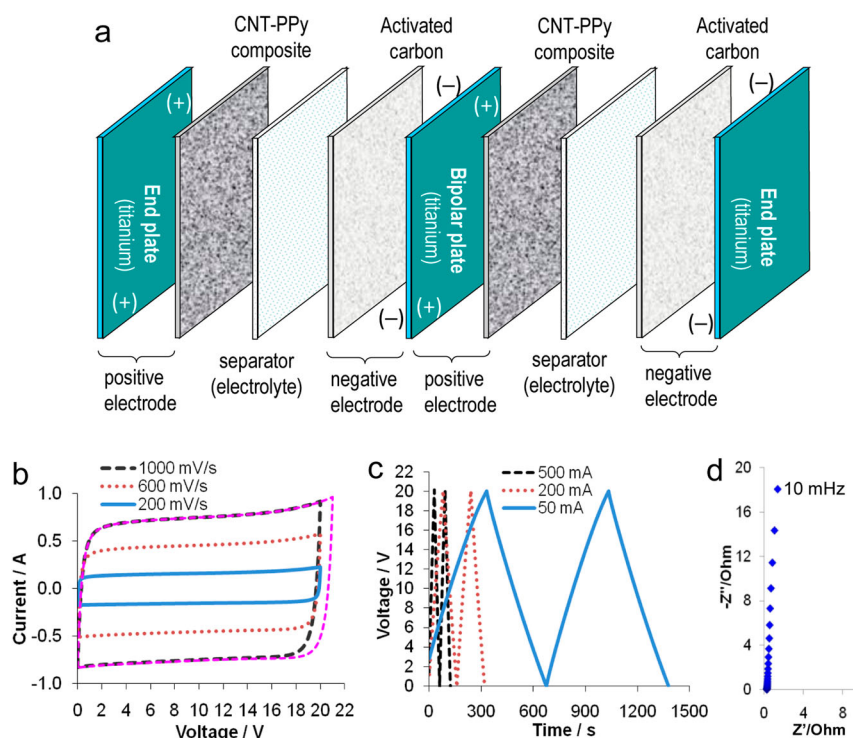


**Figure 18.** (a) Expanded schematic illustration of a stack of two 'CNT-PPy | electrolyte | activated carbon' cells (supercapacitors or supercapatteries) internally connected by a bi-polar plate (current collector) which is part of the positive electrode of the cell on the right, and part of the negative electrode of the cell on the left. CNT-PPy: composite of CNTs and polypyrrole. (b) CVs at indicated scan rates and (c) GCDs at indicated currents, and (d) ac impedance spectrum recorded on a supercapacitor stack of 19 'CNT-PPy | KCl (aqueous) | activated carbon' cells that were internally connected in series with 18 bipolar and 2 end titanium plates [71].

and negative electrodes, and to a minor degree, the use of catholyte and anolyte in places of electrolytes for the positive and negative electrodes, respectively. Four acronyms, namely, positrode (=positive electrode) and negatrode (=negative electrode), and posilyte (=electrolyte for positive electrode) and negalyte (=electrolyte for negative electrode) are proposed to promote proper and correct description of these components in EES devices. Different charge storage mechanisms are described and compared, aiming to account for the respective performance features of charge storage, particularly CVs and GCDs. These include electric double layer capacitance, pseudocapacitance (or capacitive Faradaic charge storage), and Nernstian charge storage (or non-capacitive Faradaic charge storage). In particular, the semiconductor band model has been applied to account for pseudocapacitance. Several examples are presented and discussed in relation with the synthesis, properties and charge storage performance of composites of CNTs and redox active materials, and design, fabrication and tests of devices for supercapattery. The advantages and challenges in using aqueous, organic, IL and solid ion conducting electrolytes are also analysed and compared. It is apparent that the solid ion conductors and ILs are promising for high voltage applications and hence suit supercapattery better, although their commercial use still needs further reduction in manufacturing cost. Last, but not the least, this article has provided an extended and more comprehensive definition of supercapattery.

## Funding

The author has worked with more than 20 co-workers (whose names appear in the list of references) to investigate supercapattery with financial support from the Engineering and Physical Sciences Research Council (EP/J000582/1, GR/R68078/02, GR/R68078/01), Royal Society (Braine Mercer Feasibility Award, 2006), MOSTI, E.ON AG (Energy Storage 2007), China Scholarship Council (2012–2013), Season Long Cleantech Ltd (Beijing), Ningbo Municipal People's Government (3315 Plan and the IAMET Special Fund, 2014A35001-1). Responsibility for the content of this publication lies with the author.

## ORCID

George. Z. Chen  <http://orcid.org/0000-0002-5589-5767>

## References

- [1] Larcher D, Tarascon J-M. Towards greener and more sustainable batteries for electrical energy storage. *Nat Chem*. 2014;7:19–29.
- [2] Zhang K, Han XP, Hu Z, et al. Nanostructured Mn-based oxides for electrochemical energy storage and conversion. *Chem Soc Rev*. 2015;44:699–728.
- [3] Chen GZ. Understanding supercapacitors based on nano-hybrid materials with interfacial conjugation. *Prog Nat Sci – Mater Int*. 2013;23:245–255.
- [4] Simon P, Gogotsi Y. Capacitive energy storage in nanostructured carbon–electrolyte systems. *Acc Chem Res*. 2013;46:1094–1103.
- [5] Akinwolemiwa B, Peng C, Chen GZ. Redox electrolytes in supercapacitors. *J Electrochem Soc*. 2015;162:A5054–A5059.
- [6] Hu D, Peng C, Chen GZ. Electrodeposition of non-conducting polymers: roles of carbon nanotubes in the process and products. *ACS Nano*. 2010;4:4274–4282.
- [7] Makino S, Shinohara Y, Ban T, et al. 4 V class aqueous hybrid electrochemical capacitor with battery-like capacity. *RSC Adv*. 2012;2:12144–12147.
- [8] Shimizu W, Makino S, Takahashi K, et al. Development of a 4.2 V aqueous hybrid electrochemical capacitor based on MnO<sub>2</sub> positive and protected Li negative electrodes. *J Power Sour*. 2013;241:572–577.
- [9] Panero S, Spila E, Scrosati B. On the use of ionically conducting membranes for the fabrication of laminated polymer-based redox capacitors. *J Electroanal Chem*. 1995;396:385–389.
- [10] Komatsu D, Tomai T, Honma I. Enhancement of energy density in organic redox capacitor by improvement of electric conduction network. *J Power Sources*. 2015;274:412–416.
- [11] Hung CJ, Lin P, Tseng TY. High energy density asymmetric pseudocapacitors fabricated by graphene/carbon nanotube/MnO<sub>2</sub> plus carbon nanotubes nanocomposites electrode. *J Power Sour*. 2014;259:145–153.
- [12] Conway BE, Birss V, Wojtowicz J. The role and utilization of pseudocapacitance for energy storage by supercapacitors. *J Power Sour*. 1997;66:1–14.
- [13] Sivakkumar SR, Nerkar JY, Pandolfo AG. Rate capability of graphite materials as negative electrodes in lithium-ion capacitors. *Electrochim Acta*. 2010;55:3330–3335.
- [14] Shi ZQ, Zhang J, Wang J, et al. Effect of the capacity design of activated carbon cathode on the electrochemical performance of lithium-ion capacitors. *Electrochim Acta*. 2015;153:476–483.
- [15] Bard AJ, Faulkner LR. *Electrochemical methods: fundamentals and applications*. Weinheim: Wiley; 2001.
- [16] Goodenough JB. Rechargeable batteries: challenges old and new. *J Solid State Electrochem*. 2012;16:2019–2029.
- [17] Zhang N, Liu Y-C, Chen C-C, et al. Research progress in carbon coating on LiFePO<sub>4</sub> cathode materials for lithium ion batteries. *J Electrochem*. 2015;21:201–210. Chinese.
- [18] Hermes M, Scholz F. The electrochemical oxidation of white phosphorus at a three-phase junction. *Electrochem Commun*. 2000;2:845–850.
- [19] Deng Y, Wang DH, Xiao W, et al. Electrochemistry at conductor/insulator/electrolyte three-phase interlines: a thin layer model. *J Phys Chem B*. 2005;109:14043–14051.
- [20] Xiao W, Jin XB, Deng Y, et al. Three-phase interlines electrochemically driven into insulator compounds: a penetration model and its verification by electroreduction of solid AgCl. *Chem Eur J*. 2007;13:604–612.
- [21] Conway BE, Gileadi E. Kinetic theory of pseudocapacitance and electrode reactions at appreciable surface coverage. *Trans Farad Soc*. 1962;58:2493–2509.

- [22] Hale JM, Greef R. The interpretation of adsorption pseudocapacitance curves as measured by the potential-sweep method – I. *Electrochim Acta*. 1967;12:1409–1420.
- [23] Trasatti S, Buzzanca G. Ruthenium dioxide: a new interesting electrode material. Solid state structure and electrochemical behaviour. *J Electroanal Chem Int Electrochem*. 1971;29:A1–A5.
- [24] Glarum SH, Marshall JH. The in situ ESR and electrochemical behavior of poly(aniline) electrode films. *J Electrochem Soc*. 1987;134:2160–2165.
- [25] Genies EM, Tsintavis C. Redox mechanism and electrochemical behaviour of polyaniline deposits. *J Electroanal Chem Int Electrochem*. 1985;195:109–128.
- [26] Rudge A, Davey J, Raistrick I, et al. Conducting polymers as active materials in electrochemical capacitors. *J Power Sour*. 1994;47:89–107.
- [27] Fujihira M, Matsue T, Osa T. Organo-modified metal oxide electrode. I. studies of modified layer by capacitance measurements and ESCA. *Chem Lett*. 1976;5:875–880.
- [28] Tsirlina GA, Roginskaya YE, Postovalova GG, et al. Nanostructured SnO<sub>2</sub>-TiO<sub>2</sub>, SnO<sub>2</sub>-ZrO<sub>2</sub>, and SnO<sub>2</sub>-SbO<sub>x</sub> oxides as charge-accumulating materials. *Russ J Electrochem*. 1999;35:1218–1224.
- [29] Lee HY, Goodenough JB. Supercapacitor behavior with KCl electrolyte. *J Solid State Chem*. 1999;144:220–223.
- [30] Lee HY, Goodenough JB. Ideal supercapacitor behavior of amorphous V<sub>2</sub>O<sub>5</sub>·nH<sub>2</sub>O in Potassium Chloride (KCl) aqueous solution. *J Solid State Chem*. 1999;148:81–84.
- [31] Zhang SW, Chen GZ. Manganese oxide based materials for supercapacitors. *Energy Mater*. 2008;3:186–200.
- [32] Conway BE. Transition from ‘supercapacitor’ to ‘battery’ behavior in electrochemical energy storage. *J Electrochem Soc*. 1991;138:1539–1548.
- [33] Mai L-Q, Minhas-Khan A, Tian XC, et al. Synergistic interaction between redox-active electrolyte and binder-free functionalized carbon for ultrahigh supercapacitor performance. *Nat Commun*. 2013;4, Art. No. 2923.
- [34] Wang HL, Casalongue HS, Liang YY, et al. Ni(OH)<sub>2</sub> nanoplates grown on graphene as advanced electrochemical pseudocapacitor materials. *J Am Chem Soc*. 2010;132:7472–7477.
- [35] Liu KC, Anderson MA. Porous nickel oxide/nickel films for electrochemical capacitors. *J Electrochem Soc* 1996;143:124–130.
- [36] Augustyn V, Simon P, Dunn B. Pseudocapacitive oxide materials for high-rate electrochemical energy storage. *Energy Environ Sci*. 2014;7:1597–1614.
- [37] Chae JH, Zhou XH, Chen GZ. From electrochemical capacitors to supercapatteries. *Green*. 2012;2:41–54.
- [38] Chae JH, Chen GZ. 1.9V aqueous carbon-carbon supercapacitors with unequal electrode capacitances. *Electrochim Acta*. 2012;86:248–254.
- [39] Peng C, Hu D, Chen GZ. Theoretical specific capacitance based on charge storage mechanisms of conducting polymers: Comment on ‘Vertically oriented arrays of polyaniline nanorods and their super electrochemical properties’. *Chem Commun*. 2011;47:4105–4107.
- [40] Brousse T, Belanger D, Long JW. To be or not to be pseudocapacitive? *J Electrochem Soc*. 2015;162: A5185–A5189.
- [41] Laheäär A, Przygocki P, Abbas Q, et al. Appropriate methods for evaluating the efficiency and capacitive behavior of different types of supercapacitors. *Electrochem Commun*. 2015;60:21–25.
- [42] Simon P, Gogotsi Y. Materials for electrochemical capacitors. *Nat Mater*. 2008;7:845–854.
- [43] Zheng JP, Jow TR. A new charge storage mechanism for electrochemical capacitors. *J Electrochem Soc*. 1995;142:L6–L8.
- [44] Wu MQ, Snook GA, Chen GZ, et al. Redox deposition of manganese oxide on graphite for supercapacitors. *Electrochem Commun*. 2004;6:499–504.
- [45] Wang GP, Zhang L, Zhang JJ. A review of electrode materials for electrochemical supercapacitors. *Chem Soc Rev*. 2012;41:797–828.
- [46] Peng C, Zhang SW, Jewell D, et al. Carbon nanotube and conducting polymer composites for supercapacitors. *Prog Nat Sci*. 2008;18:777–788.
- [47] Peng C, Jin J, Chen GZ. A comparative study on electrochemical co-deposition and capacitance of composite films of conducting polymers and carbon nanotubes. *Electrochim Acta*. 2007;53:525–537.
- [48] Galizzioli D, Tantardini F, Trasatti S. Ruthenium dioxide: a new electrode material. I. Behaviour in acid solutions of inert electrolytes. *J Appl Electrochem*. 1974;4:57–67.
- [49] Hu CC, Chen W-C, Chang K-H. How to achieve maximum utilization of hydrous ruthenium oxide for supercapacitors. *J Electrochem Soc*. 2004;151:A281–A290.
- [50] Zhang SW, Peng C, Ng KC, et al. Nanocomposites of manganese oxides and carbon nanotubes for aqueous supercapacitor stacks. *Electrochim Acta*. 2010;55:7447–7453.
- [51] Xiao W., Hu D., Peng C., et al. Interfacial synthesis: amphiphilic monomers assisted ultrarefining of mesoporous manganese oxide nanoparticles and the electrochemical implications. *ACS Appl Mater Interfaces*. 2011;3:3120–3129.
- [52] [http://wiki.chemprime.chemeddl.org/index.php/CoreChem:Metallic\\_Bonding](http://wiki.chemprime.chemeddl.org/index.php/CoreChem:Metallic_Bonding) (03/09/2015).
- [53] McBreen J. The electrochemistry of β-MnO<sub>2</sub> and γ-MnO<sub>2</sub> in alkaline electrolyte. *Electrochim Acta*. 1975;20:221–225.
- [54] Zhang Q-L, Yuan A-B. Nano-MnO<sub>2</sub> Activated Carbon Hybrid Supercapacitors Using Alkaline Electrolyte. *J Shanghai Univ-Nat Sci Ed*. 2006;12:624–679.
- [55] Sattar MA, Conway BE. Electrochemistry of the nickel-oxide electrode—VI. Surface oxidation of nickel anodes in alkaline solution. *Electrochim Acta*. 1969;14:695–710.
- [56] Srinivasan V, Weidner JW. Studies on the capacitance of Nickel Oxide films: effect of heating temperature and electrolyte concentration. *J Electrochem Soc*. 2000;147:880–885.
- [57] Weinert JX, Burke AF, Wei XZ. Lead-acid and lithium-ion batteries for the Chinese electric bike market and implications on future technology advancement. *J Power Sour*. 2007;172:938–945.
- [58] Duracell. Alkaline-manganese dioxide. [cited 2015 Sep 12]. [http://ww2.duracell.com/media/en-US/pdf/gtcl/Technical\\_Bulletins/Alkaline%20Technical%20Bulletin.pdf](http://ww2.duracell.com/media/en-US/pdf/gtcl/Technical_Bulletins/Alkaline%20Technical%20Bulletin.pdf).
- [59] Grande L, Paillard E, Hassoun J, et al. The lithium/air battery: still an emerging system or a practical reality? *Adv Mater*. 2015;27:784–800.

- [60] Hulicova-Jurcakova D, Seredych M, Lu GQ, et al. Combined effect of nitrogen- and oxygen-containing functional groups of microporous activated carbon on its electrochemical performance in supercapacitors. *Adv Funct Mater.* **2009**;19:438–447.
- [61] Hsieh CT, Teng H. Influence of oxygen treatment on electric double-layer capacitance of activated carbon fabrics. *Carbon.* **2002**;40:667–674.
- [62] Wu XZ, Zhou J, Xing W, et al. Insight into high areal capacitances of low apparent surface area carbons derived from nitrogen-rich polymers. *Carbon.* **2015**;94:560–567.
- [63] Griffin JM, Forse AC, Tsai W-Y, et al. In situ NMR and electrochemical quartz crystal microbalance techniques reveal the structure of the electrical double layer in supercapacitors. *Nat Mater.* **2015**;14:812–819.
- [64] Huang M, Li F, Dong F, et al. MnO<sub>2</sub>-based nanostructures for high-performance supercapacitors. *J Mater Chem A.* **2015**;3:21380–21423.
- [65] Yan J, Fan ZJ, Wei T, et al. Carbon nanotube/MnO<sub>2</sub> composites synthesized by microwave-assisted method for supercapacitors with high power and energy densities. *J Power Sour.* **2009**;194:1202–1207.
- [66] Lota K, Khomenko VK, Frackowiak E. Capacitance properties of poly(3,4-ethylenedioxythiophene)/carbon nanotubes composites. *J Phys Chem Solid.* **2004**;65:295–301.
- [67] Toupin M, Brousse T, Belanger D. Charge storage mechanism of MnO<sub>2</sub> electrode used in aqueous electrochemical capacitor. *Chem Mater.* **2004**;16:3184–3190.
- [68] He SJ, Chen W. High performance supercapacitors based on three-dimensional ultralight flexible manganese oxide nanosheets/carbon foam composites. *J Power Sour.* **2014**;262:391–400.
- [69] Jiang H, Yang L, Li C, et al. High-rate electrochemical capacitors from highly graphitic carbon-tipped manganese oxide/mesoporous carbon/manganese oxide hybrid nanowires. *Energy Environ Sci.* **2011**;4:1813–1819.
- [70] Wang HY, Yoshio M. Performance of AC/graphite capacitors at high weight ratios of AC/graphite. *J Power Sour.* **2008**;177:681–684.
- [71] Zhou XH, Peng C, Chen GZ. 20 V stack of aqueous supercapacitors with carbon (–), titanium bipolar plates and CNT-polypyrrole composite (+). *AICHE J.* **2012**;58:974–983.
- [72] Ng KC, Zhang SW, Peng C, et al. Individual and bipolarly stacked asymmetrical aqueous supercapacitors of CNTs/SnO<sub>2</sub> and CNTs/MnO<sub>2</sub> nanocomposites. *J Electrochem Soc.* **2009**;156:A846–A853.
- [73] Chen GZ., Shaffer MSP, Coleby D, et al. Carbon nanotube and polypyrrole composites: coating and doping. *Adv Mater.* **2000**;12:522–526.
- [74] Jin XB, Zhou W, Zhang SW, et al. Nanoscale microelectrochemical cells on carbon nanotubes. *Small.* **2007**;3:1513–1517.
- [75] Sassin MB, Chervin CN, Rolison DR, et al. Redox deposition of nanoscale metal oxides on carbon for next-generation electrochemical capacitors. *Acc Chem Res.* **2013**;46:1062–1074.
- [76] Kim M, Kim J. Redox deposition of birnessite-type manganese oxide on silicon carbide microspheres for use as supercapacitor electrodes. *ACS Appl Mater Interfaces.* **2014**;6:9036–9045.
- [77] Lee S-W, Bak S-M, Lee C-W, et al. Structural changes in reduced graphene oxide upon MnO<sub>2</sub> deposition by the redox reaction between carbon and permanganate ions. *J Phys Chem C.* **2014**;118:2834–2843.
- [78] Yu LP, Chen GZ. Redox electrode materials for supercapacitors. *J Power Sour.* **2016**;326:604–612.
- [79] Yu LP., Chen GZ. High energy supercapattery with an ionic liquid solution of LiClO<sub>4</sub>. *Farad Discuss.* **2016**;190:231–240.
- [80] Yang Q, Lu ZY, Liu JF, et al. Metal oxide and hydroxide nanoarrays: hydrothermal synthesis and applications as supercapacitors and nanocatalysts. *Prog Nat Sci – Mater Int.* **2013**;23:351–366.
- [81] Zhu SJ, Jia JQ, Wang T, et al. Rational design of octahedron and nanowire CeO<sub>2</sub>@MnO<sub>2</sub> core-shell heterostructures with outstanding rate capability for asymmetric supercapacitors. *Chem Commun.* **2015**;51:14840–14843.
- [82] Arul NS, Mangalaraj D, Ramachandran R, et al. Fabrication of CeO<sub>2</sub>/Fe<sub>2</sub>O<sub>3</sub> composite nanospindles for enhanced visible light driven photocatalysts and supercapacitor electrodes. *J Mater Chem A.* **2015**;3:15248–15258.
- [83] Demarconnay L, Raymundo-Pinero E, Béguin F. Adjustment of electrodes potential window in an asymmetric carbon/MnO<sub>2</sub> supercapacitor. *J Power Sour.* **2011**;196:580–586.
- [84] Cao JY, Wang YM, Zhou Y, et al. High voltage asymmetric supercapacitor based on MnO<sub>2</sub> and graphene electrodes. *J Electroanal Chem.* **2013**;689:201–206.
- [85] Peng C, Zhang SW, Zhou XH, et al. Unequalisation of electrode capacitances for enhanced energy capacity in asymmetrical supercapacitors. *Energy Environ Sci.* **2010**;3:1499–1502.
- [86] Dai ZX, Peng C, Chae JH, et al. Cell voltage versus electrode potential range in aqueous supercapacitors. *Sci Rep.* **2015**;5, Art. No. 9854.
- [87] [cited 2015 Sep 26]. <http://www.fhwa.dot.gov/publications/research/safety/95202/005.cfm> (26/09/2015).
- [88] Gao Y, Qin ZB, Guan L, et al. Organosoluble calcium chloride electrolytes for capacitive charge storage in carbon nanotubes at sub-zero-temperatures. *Chem Commun.* **2015**;51:10819–10822.
- [89] Ruan DB, Gu GS, Chen ZR, Yang B. ISEE'Cap2015. 4th Intern. Symp. on Enhanced Electrochem. Capacitors, 2015 8–12 June, Montpellier, France.
- [90] Huang B, Sun X-Z, Zhang X, et al. Organic electrolytes for activated carbon-based supercapacitors with flexible package. *Acta Phys Chim Sin.* **2013**;29:1998–2004.
- [91] Jäckel N, Weingarth D, Zeiger M, et al. Comparison of carbon onions and carbon blacks as conductive additives for carbon supercapacitors in organic electrolytes. *J Power Sour.* **2014**;272:1122–1133.
- [92] Yuan QF, Zhao FG, Wang WD, et al. Overcharge failure investigation of lithium-ion batteries. *Electrochim Acta.* **2015**;178:682–688.
- [93] Lisbona DG, Snee T. A review of hazards associated with primary lithium and lithium-ion batteries. *Process Saf Environ Protect.* **2011**;89:434–442.
- [94] Buzzeo MC, Evans RG, Compton RG. Non-haloaluminate room-temperature ionic liquids in electrochemistry - A review. *Chem Phys Chem.* **2004**;5:1106–1120.
- [95] Zhao D, Huang Q, Jin XB, et al. Capacitance at the electrode/Ionic liquid interface. *Acta Phys Chim Sin.* **2010**;26:1239–1248 (in Chinese).
- [96] Béguin F, Presser V, Balducci A, et al. Carbons and electrolytes for advanced supercapacitors. *Adv Mater.* **2014**;26:2219–2251.

- [97] Wilson BE, He SY, Buffington K, et al. Utilizing ionic liquids for controlled N-doping in hard-templated, mesoporous carbon electrodes for high-performance electrochemical double-layer capacitors. *J Power Sour.* **2015**;298:193–202.
- [98] Sato T, Masuda G, Takagi K. Electrochemical properties of novel ionic liquids for electric double layer capacitor applications. *Electrochim Acta.* **2004**;49:3603–3611.
- [99] Tan S, Ji YJ, Zhang ZR, et al. Recent progress in research on high-voltage electrolytes for lithium-ion batteries. *Chem Phys Chem.* **2014**;15:1956–1969.
- [100] Liu CG, Yu ZN, Neff D, et al. Graphene-based supercapacitor with an ultrahigh energy density. *Nano Lett.* **2010**;10:4863–4868.
- [101] Cao DX, Sun Y, Wang GL. Direct carbon fuel cell: fundamentals and recent developments. *J Power Sour.* **2007**;167:250–257.
- [102] Liu T, Leskes M, Yu WJ, et al. Cycling Li-O<sub>2</sub> batteries via LiOH formation and decomposition. *Science.* **2015**;350:530–533.
- [103] Zhou XH, Chen GZ. Unpublished results, University of Nottingham, **2012**.
- [104] Yoon Y, Lee K, Kwon S, et al. Vertical alignments of graphene sheets spatially and densely piled for fast ion diffusion in compact supercapacitors. *ACS Nano.* **2014**;8:4580–4590.
- [105] Deng X, Zhao BT, Zhu L, et al. Molten salt synthesis of nitrogen-doped carbon with hierarchical pore structures for use as high-performance electrodes in supercapacitors. *Carbon.* **2015**;93:48–58.
- [106] Padmanathan N, Shao H, McNulty D, et al. Hierarchical NiO–In<sub>2</sub>O<sub>3</sub> microflower (3D)/nanorod (1D) hetero-architecture as a supercapattery electrode with excellent cyclic stability. *J Mater Chem A.* **2016**;4:4820–4830.